EUROPEAN ORGANIZATION FOR NUCLEAR RESEARCH

CERN/EP 81-44
6 May 1981

JET-LIKE PROPERTIES OF MULTIPARTICLE SYSTEMS PRODUCED IN K^+p INTERACTIONS AT 70 GeV/c

Brussels-CERN-Genova-Mons-Nijmegen-Serpukhov Collaboration

M. Barth(*), C. De Clercq(**), E.A. De Wolf(***), J.J. Dumont(*), D.P. Johnson(**), J. Lemonne, and P. Peeters
Inter-University Institute for High Energies, Brussels, Belgium

H. Drevermann, Y. Goldschmidt-Clermont, G. Harigel, C. Milstene(+), J.P. Porte, R.T. Ross, M. Spyropoulou-Stassinaki, S. Squarcia(++) and P. Theocharopoulos
CERN, European Organization for Nuclear Research, Geneva, Switzerland

C. Caso, R. Contri, F. Fontanelli, R. Monge and U. Trevisan
Sezione INFN and Istituto di Scienze Fisiche, Genova, Italy

J.F. Baland, J. Beaufays, J. Hanton and F. Grard
Faculté des Sciences, Université de l'Etat, Mons, Belgium

L. Gatignon, W. Kittel, W.J. Metzger, P.A. van der Poel, D.J. Schotanus, A. Stergiou and R.T. Van de Walle
University of Nijmegen, Nijmegen, Netherlands

A. Borovikov, P.V. Chliapnikov, A.B. Fenyuk, L. Gerdyukov, I. Gritsaenko, O. Kasian, G. Khromova, V.M. Kubic, S. Lugovsky, V.N. Nikolaenko, Y. Petrovikh, V.M. Ronjin and V. Yarba
Institute for High Energy Physics, Serpukhov, USSR(+++)

Submitted to Nuclear Physics B

(*) Chercheur IISN, Belgium.

(**) Navorser IIKW, Belgium.

(***) Bevoegdverklaard Navorser NFWO; also at Universitaire Instelling Antwerpen.

(+) Visitor from the University of Tel-Aviv.

(++) On leave of absence from Genova University, Genova, Italy.

(+++) Participating under the terms of the 1967 Agreement between CERN and the USSR State Committee for the Utilisation of Atomic Energy and the Protocols thereto.

EP/0030P/CC/ed

ABSTRACT

We present results on the jet-like properties of multiparticle systems produced in K^+p interactions at 70 GeV/c. The data are analysed in terms of several variables commonly used to study the jet structure of an event. An extensive comparison is made with jets found in electron-positron annihilations and in deep inelastic νN interactions at comparable energy. Many similarities are found between low-p_T jets in this experiment and jets observed in leptonic interactions. Our data are very well reproduced by the Field-Feynman quark fragmentation parametrisation but equally well by a longitudinal phase space model, suggesting that these similarities do not prove or disprove the universal character of the jet fragmentation.

1. INTRODUCTION

The quark-parton picture has proved very successful in unifying our understanding of hadron production in e^+e^- annihilation [1-3], of deep inelastic $\nu(\bar{\nu})$ nucleon scattering [4-5] and high transverse momentum processes in hadron-hadron collisions [6-7]. In all these "hard" or "short distance" processes the primary interaction leaves an intermediate state containing one or more quarks (and gluons), which subsequently fragment into hadrons, forming jets of particles roughly collimated along the direction of the originating quark. This picture is supported by the experimental identification of these jets in the various hard processes and of the great similarity of (at least some of) their characteristics. At the same time these observations raise interesting questions as to the universality of jet fragmentation.

Recently, several models have attempted to extend the parton picture to hadron-hadron collisions at low p_T. These models can be conveniently classified into two groups: (i) Recombination models [8-9], which involve the parton structure functions of hadrons and (ii) fragmentation models [10-12], which relate the hadron longitudinal momentum distributions to parton fragmentation functions. Although none of these descriptions has been found fully satisfactory to reproduce all features of the data [13], they do invite further comparison in terms of parton-quark concepts.

From the experimental point of view there is accumulating evidence of striking similarities between jets in non-diffractive low p_T interactions initiated by different particles and hadronic jets observed in leptonic processes, when compared at the same total hadronic energy [14]. Using a different approach, similarities were found between charged particle production in pp interactions at the ISR and e^+e^- annihilation processes [15]. This was achieved by removing a leading proton from the system and using as the energy for comparison the remaining available hadronic energy.

In this paper, we present a comparison of the jet-like behaviour of low p_T K^+p interactions at $\sqrt{s}$ = 11.5 GeV, both with deep inelastic ν-$(\bar{\nu})$ nucleon scattering and with e^+e^- annihilations, using the

same methods of analysis as in the leptonic experiments. We also compare our results to an uncorrelated particle longitudinal phase space model and to the Field and Feynman quark fragmentation parametrisation. These comparisons allow us to draw some conclusions on the significance of the observed "universality" of jet properties.

The plan of the paper is as follows. Sect. 2 describes the data sample used for this analysis. The jet-variables and the corresponding axes are briefly discussed in sect. 3. The experimental results are described in sect. 4 and compared with data from e^+e^- annihilations and νN interactions. In sect. 5 we discuss the Field-Feynman (FF) model and the longitudinal phase space (LPS) model and compare their predictions with our data. Sect. 6 summarizes our main conclusions.

2. EXPERIMENTAL SAMPLE

The data come from an exposure of BEBC, filled with hydrogen, exposed to an r.f. separated beam of positive kaons having a nominal momentum of 70 GeV/c. Details of data taking, run conditions and cross sections have already been published [16].

The measurements were made on automatic and semi-automatic devices, and processed through the HYDRA geometry.

The present analysis is based on a partial sample of 9561 complete well measured events, having at least four charged outgoing tracks. These events correspond to a sample with the mean momentum error on the tracks $\langle \Delta p/p \rangle \simeq 2\%$ (93% of the tracks have $\frac{\Delta p}{p} < 5\%$). Events with any track with $\frac{\Delta p}{p} > 50\%$ were rejected.

All charged particles were assumed to be pions, unless identified as protons by ionization [17]. Neutral particles (K^0, Λ, $\bar{\Lambda}$ and γ) were identified by a 3-C kinematical fit [18]. The c.m. energy, $\sqrt{s}$, of these events is 11.5 GeV. The average fraction of the energy carried by charged particles is 56%, and the average fraction of the neutral energy that is observed in the neutral particles is 9%.

3. JET VARIABLE DEFINITIONS

Several variables have been proposed to describe the jet structure of multihadron events [19]. We have considered three different methods for measuring the "jetness" and determining the jet axis of an event. We express our data in terms of the following variables:

$$\text{sphericity}: \quad S = \min \frac{3}{2} \frac{\sum_j p_T^{j^2}}{\sum_j |p^j|^2} \quad ; \qquad 0. < S < 1. \tag{1}$$

$$\text{thrust}: \quad T = \max 2 \frac{\tilde{\sum}_j p_L^j}{\sum_j |p^j|} \quad ; \qquad .5 < T < 1. \tag{2}$$

$$\text{spherocity}: \quad S' = \min \left[\frac{4}{\pi} \frac{\sum_j |p_T^j|}{\sum_j |p^j|} \right]^2 \quad ; \qquad 0. < S' < 1. \tag{3}$$

where $p_L (p_T)$ is the longitudinal (transverse) momentum in the overall c.m. system with respect to the axis which either minimizes S or S' or maximizes T. Σ indicates a sum over all measured particles. In formula (2) $\tilde{\Sigma}$ stands for a summation covering the forward hemisphere only.

Sphericity is conveniently evaluated [20] by constructing from the hadron momenta the second rank tensor

$$M_{\alpha\beta} = \sum_{j=1}^{N} p_j^\alpha \, p_j^\beta \qquad (\alpha,\beta = x,y,z) \tag{4}$$

where the sum runs over all the measured particles. Let $\hat{n}_1$, $\hat{n}_2$, $\hat{n}_3$ be the unit eigenvectors of this tensor, associated with their normalized eigenvalues Q_i

$$Q_i = \frac{\sum_j (\vec{p}_j \cdot \hat{n}_i)^2}{\sum_j p_j^2} \tag{5}$$

ordered such that $Q_1 < Q_2 < Q_3$.

The principal axis (or sphericity axis) is the $\hat{n}_3$ direction; the event plane is defined by $\hat{n}_2$ and $\hat{n}_3$. The sphericity (1) is then given by

$$S = \frac{3}{2}(Q_1 + Q_2) = \frac{3}{2}(1 - Q_3) \ . \qquad (6)$$

A jet like event is expected to have $S \to 0$.

The definition of thrust as given in eq. (2) has been found to be somewhat impractical. Therefore, following ref. [21] we use

$$T = \max \frac{\sum_j |p_L^j|}{\sum_j |p_j|} \ , \qquad (7)$$

where the sum both in the numerator and in denominator now runs over all the measured particles. It is worth noting that both definitions (2) and (7) are equivalent for an event with no missing momentum. A jet-like event is expected to have $T \to 1$. To determine the thrust axis, we use the method proposed in ref. [22]; this method consists in trying as thrust axis all resultant momenta of all possible subsets of particles. As a consistency check we also tried a grid method, where a cone around the beam axis was scanned. Both methods gave consistent results for distributions and for average values.

Spherocity S' (3) was determined by the grid method, trying as spherocity axis all directions in the forward hemisphere. A jet-like event is expected to have $S' \to 0$.

4. EXPERIMENTAL RESULTS

4.1 Multiplicity distribution

It was proposed to consider the multiplicity distribution of hadron-hadron interactions in terms of two components [23]: a diffractive component assumed to be energy independent and characterized by low multiplicities, and a non-diffractive component showing an increasing multiplicity with increasing energy.

In order to compare our data to leptonic results, special attention is paid to the influence of the diffractive component. To investigate this effect in our data, we removed from our sample events having at least one leading particle with $|x| > 0.8$, where x is the Feynman variable ($x = p^*_L/p^*_{max}$). This cut affects 18.3% of the events, mainly in 4 and 6 prongs.

The average multiplicity we obtain for non-diffractive events with $n_c \geq 4$ is 7.07 ± 0.03. This value agrees with leptonic results at the same c.m. energy ($\sqrt{s} = 11.5$ GeV/c). In the forward and backward c.m. hemispheres (with respect to the beam axis) the average charged multiplicities in our data sample are equal to 3.80 ± 0.02 and 3.27 ± 0.02, respectively. The difference between the forward and backward hemispheres reflects the well-known asymmetry of inclusive x-distributions in meson-induced interactions. In fig. 1, we compare our multiplicity distribution in a KNO plot to e^+e^- results [24]. We observe a good agreement with these data, when the diffractive component is removed, whereas the corresponding distribution for the complete sample [16] (solid line on the figure) shows a different shape.

This again emphasises that the diffractive events must be removed from the sample for comparison with the leptonic data. This procedure is followed in the rest of this paper unless otherwise stated.

4.2 Determination of the jet axes

Before presenting our detailed results, we first compare how the three different methods determine the jet axis. Figs 2(a-c) show the distributions of the relative angles between the axes defined by thrust, sphericity and spherocity. The average values of this figure can give an estimate of the uncertainty in defining the jet direction. For instance, the width of the peak at half maximum in the distribution of the angle between thrust and sphericity axes is $\sim 10°$ (fig. 2(a)); this gives an estimate of the uncertainty in any quantity calculated transverse to the jet axis. The fact that our distribution is narrower than that of ref. [4] indicates that we have a better determination of the jet axis.

Fig. 2(d-f) show that the three possible jet axes are, as expected, almost equally determined by the beam direction. Moreover, we note that these distributions are similar to those of the angle between the current direction and the jet axis observed in $\bar{\nu}p$ interactions [5].

In fig. 2(g-i) we plot the correlation between the jet axis and the direction of the particle with the largest momentum. The correlation is much stronger for sphericity and spherocity than for thrust.

It is noted that if these distributions are restricted to events with small missing energy, the distributions all become narrower, peaking close to zero. The tails at large angles come from the events with large missing energy. As an example, the distribution of the angle between beam and sphericity axes is shown in fig. 2(e) for events with missing energy below 4 GeV, the average angle being $\sim 9°$ compared to $\sim 14°$ from the full sample.

Finally, we observe that our Monte-Carlo models account for most of these features. This is fully discussed in sect. 5.

4.3 Sphericity, Thrust and Spherocity distributions

In fig. 3(a), our normalized sphericity distribution is shown and compared to the data at the nearest c.m. energy obtained in e^+e^- annihilation [25] and in neutrino-(antineutrino)-proton interactions [5] at comparable hadronic energies. There is good overall agreement between our data (with diffraction removed) and the distributions from leptonic interactions. Some discrepancies appear for small sphericity values. As the diffractive events (not shown) contribute mainly to the region $S \to 0$ (and $T \to 1$, $S' \to 0$), we have studied the shape of the distribution using different definitions of the diffractive component (different x cuts, rapidity gap method). We observe that the shape of the distribution is not sensitive to the method used to remove diffractive events. Furthermore the angle between the sphericity and thrust axes indicates for small values of S (not shown) that we have a good determination of the jet axis even in this region.

Figs 4(a), 5(a) show thrust and spherocity distributions. Again, the similarity with e^+e^- and νN data is striking.

In fig. 6 we compare our <S>, 1-<T> and <S'> with selected results obtained in leptonic interactions over a wide range of energy; although slightly different definitions and reference frames were used to obtain these quantities, we observe a remarkable agreement between our data and leptonic results.

The average values of S, 1-T and S' are given in table 1. From this table one observes that the comparison of our results with those obtained using only charged particles in the final state, is justified because the two techniques do not change appreciably the average values. (We have also checked that the corresponding distributions are not affected). This is not surprising, however, because the seen neutrals are only a small fraction of the total produced neutrals.

It has been pointed out [14] that at 147 GeV/c the average values of S and T have a linear dependence on the outgoing charge multiplicity. In fig. 7 we show our <S>, <T> and <S'> as a function of the charge multiplicity and we observe that this linear relation holds true even at our energy. The results of the linear fits shown in the figure are given in table 2.

In figs 3(b), 4(b) and 5(b), we compare our data with the predictions of the Field Feynman and Longitudinal Phase Space models, fully discussed in sect. 5. The two models describe the data very well and yield very similar predictions. The models also predict the linear dependence of <S>, <T> and <S'> on the charge multiplicity suggesting that the dependence is of kinematical origin.

4.4 Single-particle distributions

In hadron collisions, the limitation of the particle momentum transverse to the jet (or beam) axis is one of the best-known universal characteristics of these interactions. The same phenomenon is observed in hard scattering processes at present energies.

Fig. 8 shows the normalized p_T^2 distribution of all measured particles relative to the sphericity axis. It agrees well with the e^+e^- [TASSO] data [3] (where only charged particles were measured) for $p_T^2 < 0.5$ (GeV/c)^2. At higher p_T^2, the TASSO data are slightly but systematically above our data. This excess is most probably due to the higher energy, used for the comparison.

In addition to the limitation of $\langle p_T \rangle$, the mean particle momentum transverse to the jet axis, a characteristic feature of hadronic jets is the increase of the mean longitudinal momentum $\langle p_L \rangle$, with increasing energy. These quantities relative to the thrust axis, given in table 3, are shown in fig. 9 together with PLUTO data [26]. To suppress the non-scaling part of the single particle distribution [32], we show also $\langle p_L \rangle$ with $x = 2p^*_{/\!/}/E_{cm} > 0.1$. This quantity shows a linear rise with c.m. energy while the transverse momentum shows little change with energy. From $\langle p_T \rangle$ and $\langle p_L \rangle$ we can estimate the average opening angle of particles in a jet to be $\sim 25°$ (for the half opening angle), in agreement with the corresponding value found in e^+e^- at 9.4 GeV [21].

The normalized rapidity distribution, $\frac{1}{\sigma}\frac{d\sigma}{dy}$, of charged particles, in the overall c.m., evaluated with respect to the thrust axis is shown in fig. 10. To avoid the asymmetry due to the backward identified protons, we use here only particles produced forward in the total c.m. The TASSO results at c.m. energy 13 GeV, to which our data are compared, refer only to charged particles, assumed to be pions. Our distribution has a dip at $y \sim 0$, as expected, since the thrust axis is rotated relative to the beam by a small amount, such that tracks close to y = 0 with respect to the beam acquire a longitudinal component with respect to the thrust. The plateau at $0.2 \leq y \leq 1.0$ is in good agreement with e^+e^- data. Moreover, we note (insert of fig. 10) that our K^+p data follow the linear increase with $\ln E_{cm}$ for the height of the plateau found in e^+e^-.

Finally, in fig. 11 we present the average p_T^2 as a function of x in the two hemispheres, calculated with respect to the thrust axis. The forward jet appears to be "wider", an effect which is usually interpreted in terms of planar events. This p_T broadening, however, is essentially due to positive and neutral particles, as can be derived by comparing the

effect with the symmetric distribution obtained using only negative particles in the jet (open points). A possible alternative explanation is therefore that this broadening effect can be due to resonances produced diffractively.

4.5 Jet shape analysis

The "shape" of events in momentum space can be investigated using a large number of "collective" variables.

In fig. 12 we present the energy-flow angular distribution, $\frac{1}{E_{tot}} \frac{dE}{d\lambda}$ where λ is the angle of each particle with respect to the thrust axis, for all measured particles, in three intervals of thrust. As expected, the energy flow is strongly correlated with the thrust value, the distribution becoming wider as the events become more "spherical".

This correlation can also be seen from fig. 13 where $\langle\lambda\rangle$, weighted with energy, is given as a function of T. A very similar correlation is observed in e^+e^- data [21] and in antineutrino proton interactions for $W > 4.5$ GeV [5].

The jet event shape can be expressed in terms of the normalized eigenvalues [5] of the sphericity tensor.

The average values of the three eigenvalues are presented in table 4, together with the ratio $\langle Q_1/Q_2 \rangle$ which gives an estimate of the planarity of the events. The meaning of these eigenvalues can be summarized in the following way:

(i) Q_3 estimates the length of the event,
(ii) Q_2 estimates the width of the event,
(iii) Q_1 estimates the flatness of the event.

Our diffractive events are more "jet-like" as expected; the apparent larger planarity effect in this sample is probably due to the almost random choice obtained ordering small values of Q_1 and Q_2.

Since we are dealing with normalized eigenvalues, (namely $Q_1 + Q_2 + Q_3 = 1$) each event can be represented in a Dalitz-like equilateral triangle of unit height. However, the ordering restricts the allowed region to only a sixth of this triangle. Fig. 14 shows our events in terms of the two independent variables $x = \frac{3}{2}(Q_1 + Q_2)$ and $y = \frac{\sqrt{3}}{2}(Q_2 - Q_1)$.

The bulk of the data is accumulated near $Q_3 \sim 1$, $Q_1 \sim Q_2 \sim 0$ ("cigar" shaped events). However, we observe also that some events have a coplanar behaviour ($Q_1 \sim 0$, $Q_2 \neq 0$). The question arises whether this planarity effect represents a real effect or just the "tail" of the two back-to-back jets. A more detailed study of these planar events can be obtained separating the momentum perpendicular to the jet axis into two components

$$\langle p_T^2 \rangle_{out} = \frac{1}{N} \sum_{j=1}^{N} (\vec{p}_j \cdot \hat{n}_1)^2 \tag{8}$$

$$\langle p_T^2 \rangle_{in} = \frac{1}{N} \sum_{j=1}^{N} (\vec{p}_j \cdot \hat{n}_2)^2 \tag{9}$$

$\langle p_T^2 \rangle_{out}$ is the square of the momentum component normal to the event plane, while $\langle p_T^2 \rangle_{in}$ is the square of the momentum component in the event plane perpendicular to the jet axis. A planar effect, if any, should appear in the $\langle p_T^2 \rangle_{in}$ distribution, while $\langle p_T^2 \rangle_{out}$ should be approximately the same for planar and non-planar events. Fig. 15 shows the $\langle p_T^2 \rangle_{out}$ and $\langle p_T^2 \rangle_{in}$ distributions. Our data are in very good agreement with e^+e^- data [25], and the extension to higher values of $\langle p_T^2 \rangle_{in}$ is probably due to the larger statistics. Furthermore, the prediction of FF or LPS accounts for most of the tail of the $\langle p_T^2 \rangle_{in}$ distribution, indicating that this planar effect, if present, is very marginal at our energy.

Fig. 16 shows the planarity and the flatness, defined as

$$P = Q_2 - Q_1 \tag{10}$$

and

$$F = 1 - Q_1/Q_2 \tag{11}$$

We do not observe a significant excess of events for large values of P or small values of F (planar event), the data being fairly well reproduced by the predictions of FF and LPS.

Another coordinate system has been proposed in ref. [27]. This coordinate system is defined by the Thrust axis (7), the Major axis $\hat{e}_2$, which is the direction along which the sum of the projected momenta in the plane perpendicular to the thrust axis is maximized:

$$\text{Major} = \max \frac{\Sigma |\vec{p}_j \cdot \hat{e}_2|}{\Sigma |p_j|} \qquad (12)$$

and the Minor axis, which is orthogonal to the thrust and the major axes. The difference Major - Minor called oblateness, is an estimate of the planarity of the event. The distribution of the Oblateness is given in fig. 19, together with the predictions of FF and LPS. We observe a small excess of events with large Oblateness.

4.6 Comparisons using systems with a leading proton removed

It has been shown [15] that in pp interactions, once the effect of the leading proton has been removed, the distributions agree with those found in e^+e^- annihilation.

Fig. 18 shows the dependence of the average charged multiplicity on the total hadron energy for several types of interactions (the figure has been adapted from ref. [15]). The ISR data [15] were obtained by subtracting from the total energy the energy of the "leading proton". The agreement with e^+e^- data indicates that the remaining available energy for particle production is the appropriate variable. We applied a similar method to determine the mean charged multiplicity in the backward hemisphere, where a cut $-0.8 < x < -0.4$ removes $\sim$ 80% of the identified protons. This x-cut, and the rejection of "diffractive events", corresponds to a backward remaining energy E_{had} in the range 1-3.5 GeV, with an average value of $\sim$ 2.23 GeV (in this context, E_{had} is defined as $E_{CM}/2 - E_{leading}$). The average charged multiplicities (multiplied by a factor of two and compared to e^+e^- interactions having twice E_{had} in their c.m.) are also shown in fig. 18 at our different hadronic energies. The agreement with the other data is excellent.

Similar good agreement is observed in fig. 19 where the normalized x_R distributions, $1/\sigma(d\sigma/dx_R)$, where $x_R = P/E_{had}$, are shown for two energy intervals E_{had} = 1-2 GeV and 2-3 GeV and compared to SPEAR e^+e^- data at $\sqrt{s} \sim 2E_{had}$.

5. COMPARISON WITH JETS MODELS

The experimental data, presented in previous sections, were systematically compared with the Field and Feynman (FF) jet model [28,29] and with an uncorrelated particle model, referred to as the LPS model [30].

For the first model, two back-to-back jets were generated allowing u or $\bar{s}$ from the projectile and u or d (u twice as frequently as d) from the target to fragment into mesons. The fragmentation process involves three main parameters [28]:

(a) σ_q which determines the transverse momentum of the quarks;

(b) P/V which fixes the fraction of pseudoscalar to vector mesons produced in the cascade;

(c) a_F which determines the fragmentation function of a quark into hadrons.

In order to reproduce the p_T^2 distribution relative to the jet axis (fig. 8), the σ_q was increased from its value of 250 MeV/c in ref. [28] to 300 MeV/c. This modification was also found necessary in ref. [25]. For the other parameters, P/V and a_F, the values given in ref. [28] were used (P/(P + V) = 0.5, a_F = 0.77). We note that the FF Monte-Carlo reproduces quite well the measured charged multiplicity (most sensitive to the ratio P/V).

All generated events were analysed in the same way as the experimental data. We found that the different jet-axes defined by eqs (1), (7) and (3) deviate from the original quark direction by an average angle of about 10°, which is about the uncertainty observed in figs 2.

In the LPS model, n particle exclusive final states were generated [31] according to the following matrix element:

$$|M|^2 = \prod_{i=1}^{n} \exp[-B(y_i)m_T^i] \qquad (13)$$

where m_T^i is the transverse mass ($m_T = \sqrt{p_T^2 + m^2}$) of particle i, calculated with respect to the beam direction; $B(y_i)$ is a rapidity dependent parameter taken from the experimental data [32]. The various exclusive reactions, containing $\pi^{\pm}$, π^0, K^0, protons and neutrons were properly weighted using measured average charged and neutral multiplicities. From figs 2(d-f) we observe that this model describes well the distribution of the relative angle between the jet axes and the beam direction. Since the model is constructed with the jet axis along the beam direction, this result shows that the "true" jet axis in the bulk of low-p_T events is indeed the beam axis. The angular distribution of the reconstructed jet-axis originates from (a) the intrinsic fluctuation from event-to-event, generated by the transverse momentum distribution, (b) the lack of energy-momentum conservation due to undetected neutral particles. Both effects affect somewhat differently the jet-algorithms described in sect. 3.

The predictions of the two models were already discussed in previous sections. In general, very good agreement with the data is found. Further comparison of the models, both among themselves and with the data leads us to several observations. In the LPS model, both multiplicity and transverse momentum distributions are chosen to describe the experimental data. The successes of the LPS model show that these two ingredients are sufficient to describe the data.

In the FF model, definite mechanisms of quantum-number flow are incorporated in the fragmentation process that leads to a hadron jet. However when jet-properties are averaged over (additive) quantum numbers, quantum-number correlations become irrelevant. In addition, comparison of the two models demonstrates that short-range correlations (e.g. due to resonances), included in the FF-model, but absent in the LPS-model, as well as detailed structure of the longitudinal momentum distributions have essentially no influence on the behaviour of the "collective" variables (1), (7) and (3).

Returning to comparisons between the experimental data, it was shown in sect. 4 that (a) the average charge multiplicity in non-diffractive low p_T hadronic interactions and in leptonic processes are similar at the same c.m. energy; (b) the transverse momentum distribution, with respect to the jet axis, is also similar. We conclude from the Monte-Carlo models that the remarkable similarity of many characteristics of "soft" and "hard" jets originates from (a) and (b).

This fact allows us to appreciate further the interpretation of our results. Indeed, the "universality" now traced to the similarities in average multiplicity and transverse momentum distribution, is not sufficient to show fundamental similarities between low p_T hadronic dynamics and the leptonic processes. Moreover it remains to be seen whether these observations [(a) and (b)] are still valid at higher energies where perturbative QCD effects become more prominent in leptonic processes. The lack of sensitivity of most of the collective variables used, indicates that other methods are needed to prove or disprove the "universal" character of jet fragmentation. Quantum-number content and quantum-number flow are possible candidates.

CONCLUSIONS AND SUMMARY

We have done an extensive comparison of low-p_T "jets" in non-diffractive K^+p interaction at $\sqrt{s}$ = 11.5 GeV with jets found in e^+e^- annihilations and in $\nu(\bar{\nu})N$ interactions at similar energies. We find a good overall agreement between the collective properties of these two classes of jets when compared at the same hadronic c.m. energy. Agreement is also found when comparing various inclusive single particle distributions. In particular the transverse momentum distribution and the average charge multiplicity are very similar.

Our data were compared to the predictions of two Monte-Carlo models (LPS and FF). Both models describe the data equally well, and yield very similar predictions. This is not unexpected since the input to the models is essentially the same, namely the average charged particle multiplicity and transverse momentum distribution. We conclude that these two features account for many of the other similarities observed.

Thus other methods are required to prove or disprove the "universal" character of the jet fragmentation process, such as quantum number content or flavour-flow.

Acknowledgements

It is a pleasure to thank our scanning and measuring staff at our respective laboratories and the operating crews of BEBC and the SPS accelerator, and members of the EF division for their help with the RF beam.

REFERENCES

[1] G. Hanson et al., Phys. Rev. Letters 35 (1975) 196;
G. Hanson, Proc. 18th Int. Conf. on High Energy Phys., Tbilisi, USSR, 1976 (Dubna 1977); SLAC-PUB-1814 (1976).

[2] Ch. Berger et al., PLUTO Collaboration, Phys. Letters 86B (1979) 418; DESY Report 79/57.

[3] R. Brandelik et al., TASSO Collaboration, Phys. Letters 86B (1979) 243; DESY Report 79/53.

[4] K.W.J. Barnham et al., Phys. Lett. 85B (1979) 300.

[5] M. Derrick et al., Phys. Letters 88B (1979) 177.

[6] M. Della Negra et al., Nucl. Phys. B127 (1977) 1.

[7] C. Bromberg et al., Phys. Rev. Letters 38 (1977) 1447.

[8] L. Van Hove, S. Pokorski, Nucl. Phys. B86 (1975) 243;
W. Ochs, Nucl. Phys. B118 (1977) 397;
G. Cohen-Tannoudji, A. El Assouni, J. Kalinowski and R. Peschanski, SACLAY Preprint DPh-T/78/88 (1978).

[9] K.P. Das and R.C. Hwa, Phys. Lett. 68B (1977) 549;
R.C. Hwa and R. Roberts, Zeitschr. Physik C1 (1979) 89.

[10] B. Andersson, G. Gustafson and C. Peterson, Phys. Lett. 69B (1977) 221 and Phys. Lett. 71B (1977) 337.

[11] A. Capella, U. Sukhatme, J. Tran Thanh Van, Z. Physik C3 (1980) 329;

[12] G. Cohen-Tannoudji, A. El Hassouni, J. Kalinowski, O. Napoly and R. Peschanski, SACLAY Preprint DPh-T/79/92 (1979).

[13] U. Sukhatme, Proc. XIV Rencontre de Moriond (ed. J. Tran Thanh Van 1979); ORSAY Preprint LPTPE 79/19 (1979).
R. Göttgens et al., CERN/EP 80-102, submitted to Particles and Fields.

[14] R. Göttgens et al., Nucl. Phys. B178 (1981) 392;
D. Brick et al., International Hybrid Spectrometer Consortium, IFNUP/AE01/81 submitted for publication to Nuovo Cimento.

[15] M. Basile et al., Phys. Lett. 92B (1980) 367, Nuovo Cimento 58A (1980) 193, Phys. Lett. 95B (1980) 311 and Lett. Nuovo Cimento 29 (1980) 491.

[16] M. Barth et al., Z. Physik C, Particles and Fields 2 (1979) 285.

REFERENCES (Cont'd)

[17] M. Barth et al., Z. Physik C, Particles and Fields 7 (1981) 89.

[18] M. Barth et al., Inclusive K^0 and K^{*+} Production in 70 GeV/c K^+p Interactions, CERN/EP 80-105.

[19] S. Brandt and H.D. Dahmen, Z. Physik C, Particles and Fields 1 (1979) 61.

[20] M. Counihan, Phys. Lett. 59B (1975) 367.

[21] Ch. Berger et al., PLUTO Collaboration, Phys. Lett. 78B (1978) 176.

[22] S. Brandt et al., Phys. Lett. 12 (1964) 57.

[23] H. Harari and E. Rabinovici, Phys. Lett. 43B (1973) 49;
K. Fialkowski and H.I. Miettinen, Phys. Lett. 43B (1973) 61;
L. Van Hove, Phys. Lett. 43B (1973) 65;
A. Wroblewski, Acta Phys. Pol. B4 (1973) 857;
N. Schmitz, Acta Phys. Pol. B4 (1973) 689.

[24] Ch. Berger et al., PLUTO Collaboration, Phys. Lett. 95B (1980) 313.

[25] R. Brandelik et al., TASSO Collaboration, Z. Physik C, Particles and Fields 4 (1980) 87 and DESY Rep. 79/74.

[26] Ch. Berger et al., PLUTO Collaboration, Phys. Lett. 81B (1979) 410.

[27] D.P. Barber et al., MARKJ Collaboration, Phys. Rev. Lett. 43 (179) 830.

[28] R.D. Field and R.P. Feynman, Nucl. Phys. B136 (1978) 1.

[29] B. Andersson et al., Z. Physik C, Particles and Fields 1 (1979) 105.

[30] L. Van Hove, Rev. Mod. Phys. 36 (1964) 655.
E.H. de Groot and T.W. Ruijgrok, Nucl. Phys. B101 (1975) 95.

[31] D. Drijard, GENLON, CERN Computer Centre Program Library.

[32] M. Barth et al., Z. Physik C, Particles and Fields 7 (1981) 187.

TABLE CAPTIONS

Table 1 Average values of S, 1-T and S' for different sets of data. For sake of completeness, we give also average values obtained with the definition given in ref. [4], where the spherocity and thrust axes are the direction of the resultant four-momentum vectors of hadrons that travel forward in the measured hadrons c.m.s. (Statistical errors only).

Table 2 Coefficients of the straight line fits to $\langle S \rangle$, $\langle T \rangle$ and $\langle S' \rangle$ as a function of the charge multiplicity. The fits are shown in fig. 7.

Table 3 Average values of $\langle p_L \rangle$, $\langle p_T \rangle$, $\langle p_T^2 \rangle$ with respect to the thrust axis for different sets of data. (Statistical errors only).

Table 4 Average values of the eigenvalues Q_i and of the ratio Q_1/Q_2 for different sets of data. (Statistical errors only).

TABLE 1

		<Sphericity>	1-<Thrust>	<Spherocity>
All particles (charged + neutrals)	All events	0.186 ± 0.002	0.138 ± 0.001	0.212 ± 0.002
	Non-diffractive events	0.221 ± 0.002	0.158 ± 0.001	0.249 ± 0.002
	Diffractive events	0.026 ± 0.001	0.046 ± 0.001	0.041 ± 0.001
	As in ref. [4], diffraction removed		0.170 ± 0.001	0.314 ± 0.003
Charged particles only	All events	0.185 ± 0.002	0.136 ± 0.001	0.207 ± 0.002
	Non-diffractive events	0.220 ± 0.002	0.156 ± 0.001	0.244 ± 0.002
	Diffractive events	0.024 ± 0.001	0.045 ± 0.001	0.039 ± 0.001
	As in ref. [4], diffraction removed		0.169 ± 0.001	0.311 ± 0.003

TABLE 2

Fits of straight line $y = an_c + b$

	a	b	χ^2/NDF
Sphericity	.0282 ± .0008	.021 ± .005	1.31
Thrust	-.0166 ± .0004	.959 ± .003	0.50
Spherocity	.0345 ± .0007	.005 ± .005	0.44

TABLE 3

		$\langle p_L \rangle$	$\langle p_L \rangle_{x_{/\!/} > .1}$	$\langle p_T \rangle$	$\langle p_T^2 \rangle$
All particles (charged + neutral)	All events	.866 ± .004	1.614 ± .009	.322 ± .001	.159 ± .001
	Non-diffractive events	.731 ± .004	1.433 ± .007	.327 ± .001	.163 ± .001
	Diffractive events	1.811 ± .021	2.436 ± .032	.290 ± .002	.133 ± .002
Charged particles only	All events	.899 ± .004	1.629 ± .009	.327 ± .001	.160 ± .001
	Non-diffractive events	.753 ± .004	1.437 ± .008	.332 ± .001	.164 ± .001
	Diffractive events	1.883 ± .022	2.481 ± .033	.294 ± .002	.135 ± .002

TABLE 4

	Non-diffractive events	Diffractive events	All events
$\langle Q_3 \rangle$	0.853 ± 0.001	0.983 ± 0.001	0.876 ± 0.001
$\langle Q_2 \rangle$	0.112 ± 0.001	0.014 ± 0.001	0.094 ± 0.001
$\langle Q_1 \rangle$	0.0352 ± 0.0005	0.0030 ± 0.0002	0.0295 ± 0.0005
$\langle Q_1/Q_2 \rangle$	0.329 ± 0.002	0.237 ± 0.005	0.312 ± 0.002

FIGURE CAPTIONS

Fig. 1 KNO plot for non-diffractive events. The solid curve corresponds to the full sample. e^+e^- data are from ref. [24].

Fig. 2 Distributions of the angles between the following different axes

(a) Thrust and sphericity.
(b) Thrust and spherocity.
(c) Sphericity and spherocity.
(d) Thrust and beam.
(e) Sphericity and beam.
(f) Spherocity and beam.
(g) Thrust and fastest particle.
(h) Sphericity and fastest particle.
(i) Spherocity and fastest particle.

The open points in (e) refer to events with missing energy below 4 GeV. The superimposed curves are the expected distributions from FF (dashed lines) and from LPS (continuous line).

Fig. 3 (a) Sphericity distribution for non-diffractive data. e^+e^- data are from ref. [25] and $\nu(\bar{\nu})p$ data from ref. [5].

(b) Same as in (a). The superimposed curves are the expected sphericity distributions from FF (dashed line) and from LPS (continuous line).

Fig. 4 (a) Thrust distribution for non-diffractive data. e^+e^- data are from ref. [25] and νN data from ref. [4].

(b) Same as in (a). The superimposed curves are the expected thrust distributions from FF (dashed line) and from LPS (continuous line).

FIGURE CAPTIONS (Cont'd)

Fig. 5 (a) Spherocity distribution for non-diffractive data. νN data are from ref. [4].

(b) Same as in (a). The superimposed curves are the expected spherocity distributions from FF (dashed line) and from LPS (continuous line).

Fig. 6 (a) $\langle S \rangle$ as a function of $\sqrt{s}$ compared with e^+e^- [21,25] and νN [4] data. The curve is a parametrization taken from ref. [25].

(b) $1-\langle T \rangle$ as a function of $\sqrt{s}$ compared with e^+e^- [21,25] and νNe [4] data.

(c) $\langle S' \rangle$ as a function $\sqrt{s}$ compared with νNe [4] data.

Fig. 7 (a) Average sphericity.
(b) Average thrust.
(c) Average spherocity.

as a function of the charge multiplicity. The coefficients of the fitted straight lines are listed in table 2.

Fig. 8 $1/\sigma \; d\sigma/dp_T^2$ as a function of p_T^2 relative to the sphericity axis. The e^+e^- data are from ref. [3]. The superimposed curves are the expected p_T^2 distributions from FF (dashed line) and from LPS (continuous line).

Fig. 9 Average observed parallel and transverse momentum with respect to the thrust axis. The triangle data points are obtained for $\langle p_L \rangle$ with $x = 2p_{/\!/}/E_{cm} > 0.1$. The e^+e^- data are from ref. [26].

FIGURE CAPTIONS (Cont'd)

Fig. 10 (a) Rapidity distribution $1/\sigma\ d\sigma/dy$ for non diffractive events (using thrust axis). We use here only charged particles produced in the c.m. forward hemisphere. In the insert, rapidity distribution $1/\sigma\ d\sigma/dy$ averaged over $0.2 < y < 1$ as a function of the c.m. energy.

Fig. 11 $\langle p_T^2 \rangle$ as a function of x in the two hemispheres (forward and backward). $\langle p_T^2 \rangle$ is calculated with respect to the thrust axis. Points refer to seen particles, open points to negative particles only.

Fig. 12 Angular distributions $(1/E_{TOT}\ dE/d\lambda)$ of observed particles with respect to the thrust axis for thrust intervals 0.85 - 1.0, 0.75 - 0.85 and 0.5 - 0.75.

Fig. 13 Correlation between the width of the energy flow distribution and the thrust value.

Fig. 14 Plot of $y = \frac{\sqrt{3}}{2}(Q_2 - Q_1)$ versus $x = \frac{3}{2}(Q_1 + Q_2)$ for the non-diffractive sample. The lines indicate the kinematical boundaries.

Fig. 15 (a) $\langle p_T^2 \rangle_{out}$ distribution.

(b) $\langle p_T^2 \rangle_{in}$ distribution (see text for the definitions). In both figures the e^+e^- data at W = 13 - 17 GeV are entered [25]. The superimposed curves are the expected distributions from FF (dashed curve) and from LPS (continuous curve), respectively.

FIGURE CAPTIONS (Cont'd)

Fig. 16 (a) Planarity distribution.

(b) Flatness distribution (see text for the definitions). The curves are the predictions of FF (dashed curve) and LPS (continuous curve), respectively.

Fig. 17 Oblateness distribution (see text for the definition). The curves are the predictions of FF (dashed curve) and LPS (continuous curve), respectively.

Fig. 18 Mean charged multiplicity (obtained doubling the mean charged multiplicity in the backward hemisphere) as compared with e^+e^- and pp data.

Fig. 19 $1/\sigma\ d\sigma/dx_R$ in the backward hemisphere for charged particles. Our data, for two different ranges of E_{had}, are compared with e^+e^- data [1] having $\sqrt{s}$ comparable with $2E_{had}$.

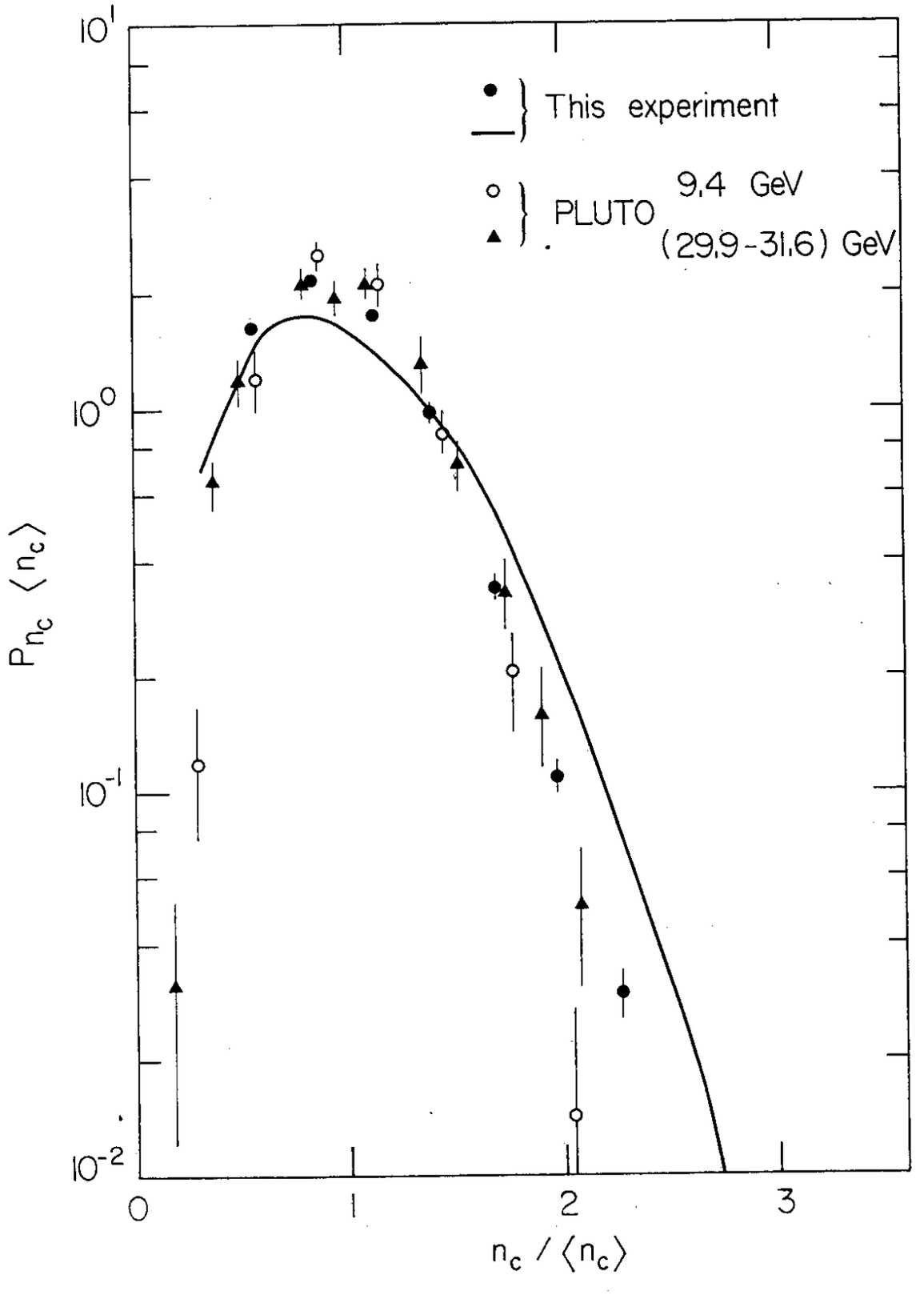
This experiment
PLUTO
9.4 GeV
(29.9-31.6) GeV
$P_{n_c}\langle n_c\rangle$
$n_c / \langle n_c\rangle$
10^1
10^0
10^{-1}
10^{-2}
0
1
2
3

Fig. 1

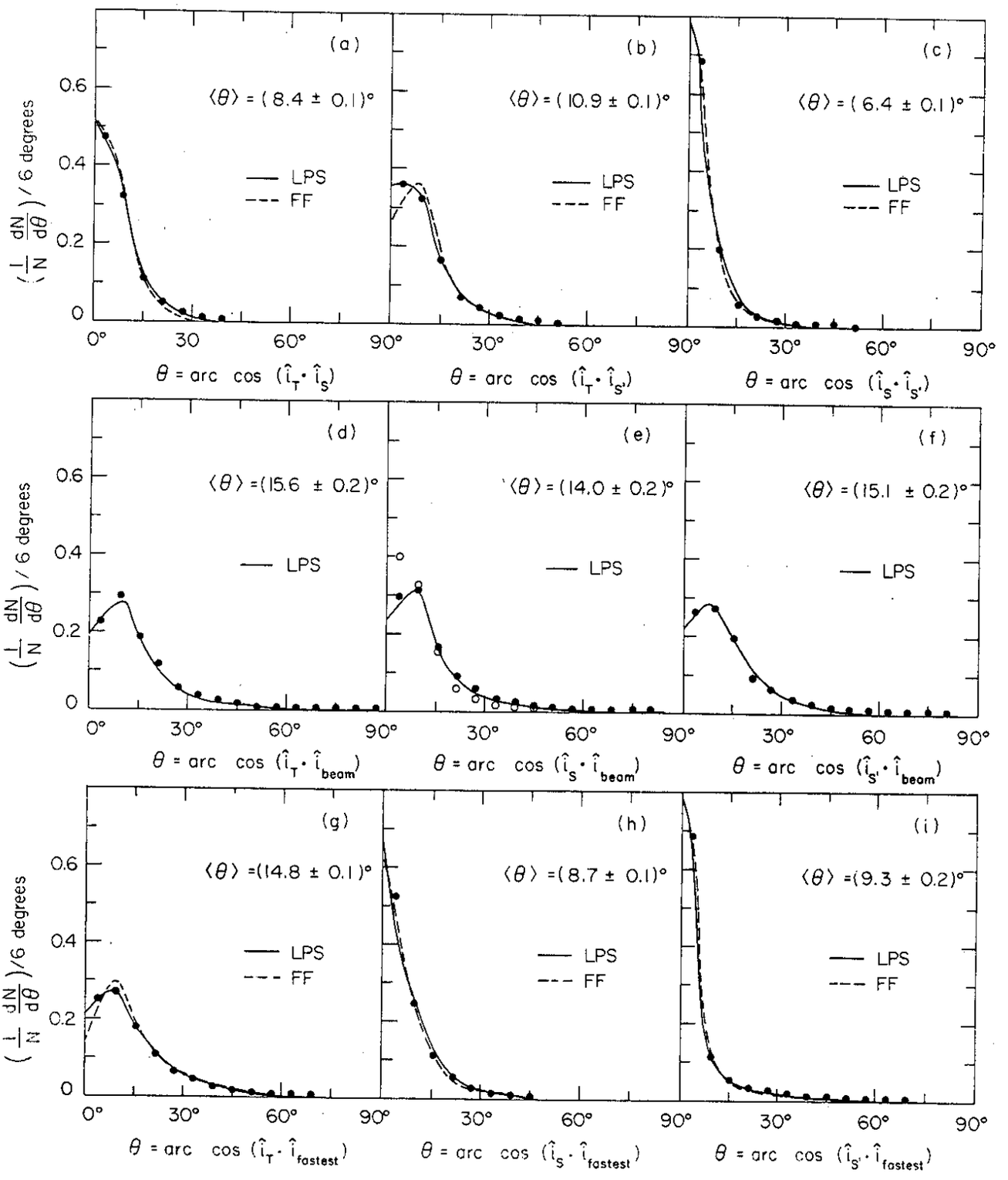
(a)
⟨θ⟩ = (8.4 ± 0.1)°
LPS
FF
(b)
⟨θ⟩ = (10.9 ± 0.1)°
LPS
FF
(c)
⟨θ⟩ = (6.4 ± 0.1)°
LPS
FF
(d)
⟨θ⟩ =(15.6 ± 0.2)°
LPS
(e)
⟨θ⟩ = (14.0 ± 0.2)°
LPS
(f)
⟨θ⟩ = (15.1 ± 0.2)°
LPS
(g)
⟨θ⟩ =(14.8 ± 0.1)°
LPS
FF
(h)
⟨θ⟩ =(8.7 ± 0.1)°
LPS
FF
(i)
⟨θ⟩ =(9.3 ± 0.2)°
LPS
FF
(1/N dN/dθ) / 6 degrees
θ = arc cos (î_T · î_S)
θ = arc cos (î_T · î_S')
θ = arc cos (î_S · î_S')
θ = arc cos (î_T · î_beam)
θ = arc cos (î_S · î_beam)
θ = arc cos (î_S' · î_beam)
θ = arc cos (î_T · î_fastest)
θ = arc cos (î_S · î_fastest)
θ = arc cos (î_S' · î_fastest)

Fig. 2

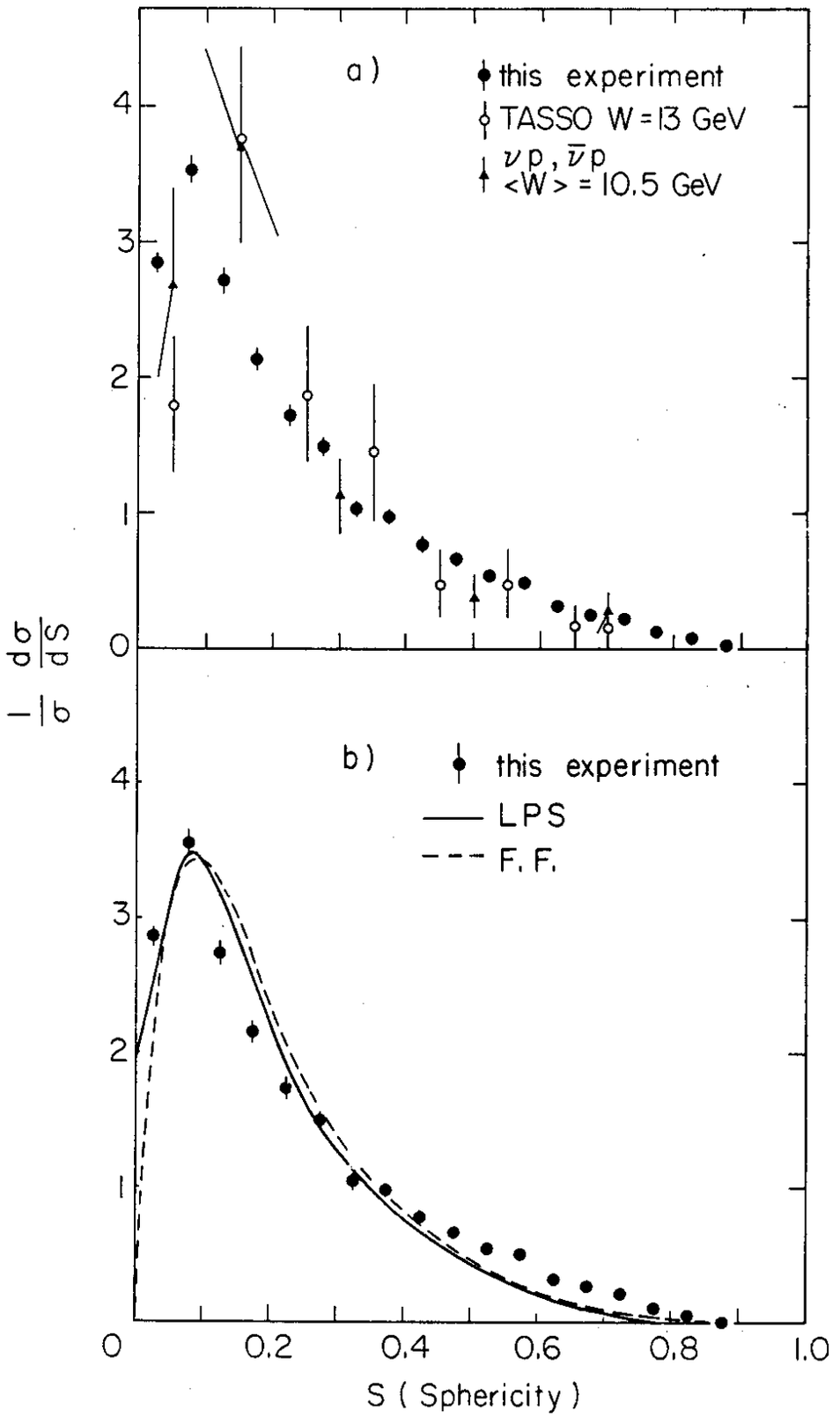
a)
this experiment
TASSO W = 13 GeV
$\nu p, \bar{\nu} p$
$\langle W \rangle$ = 10.5 GeV
b)
this experiment
LPS
F. F.
$\frac{1}{\sigma}\frac{d\sigma}{dS}$
S (Sphericity)
0
0.2
0.4
0.6
0.8
1.0
1
2
3
4

Fig. 3

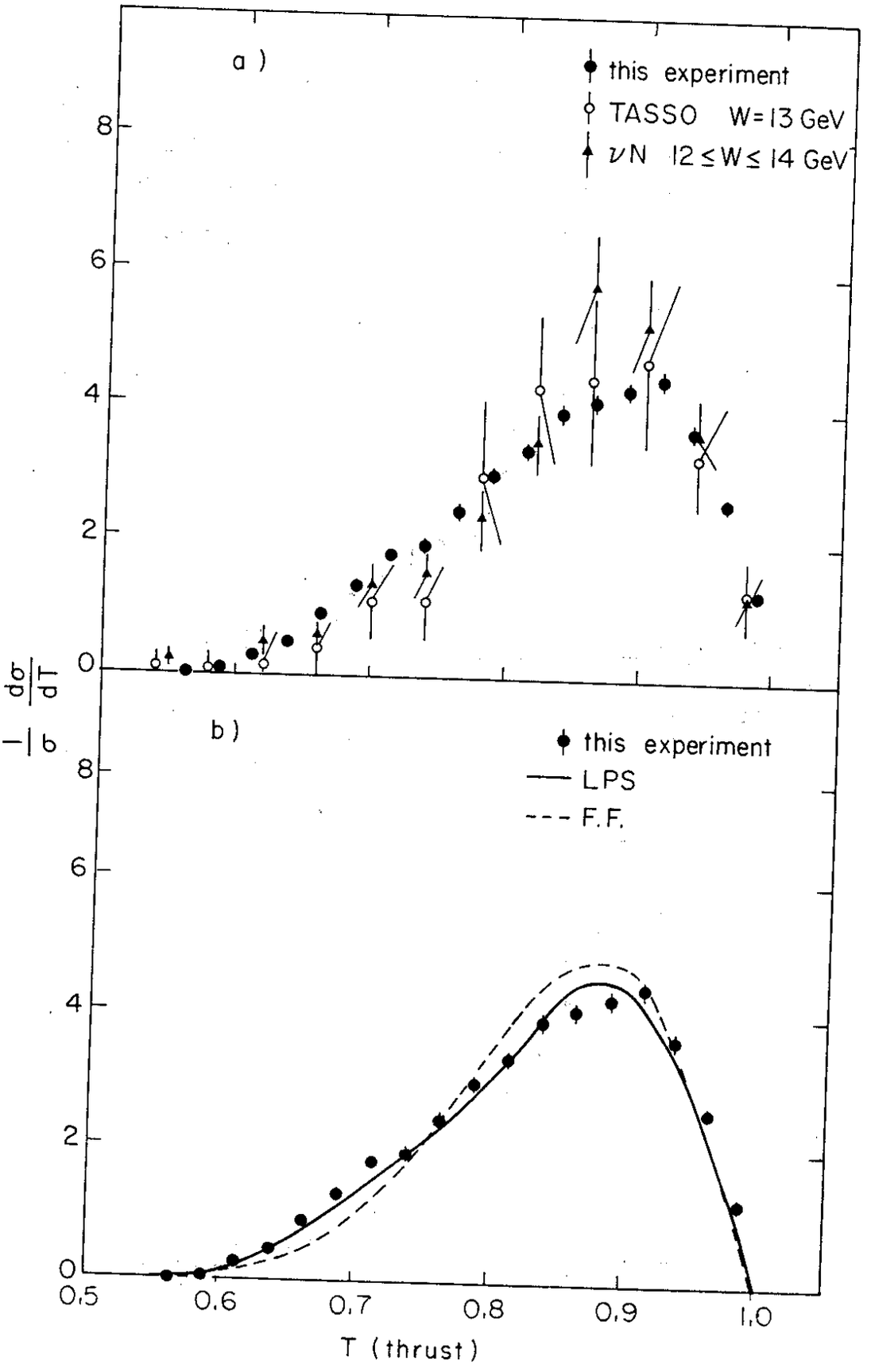
a)
this experiment
TASSO W=13 GeV
νN 12 ≤ W ≤ 14 GeV
b)
this experiment
LPS
F.F.
1/σ dσ/dT
T (thrust)
0
2
4
6
8
0.5
0.6
0.7
0.8
0.9
1.0

Fig. 4

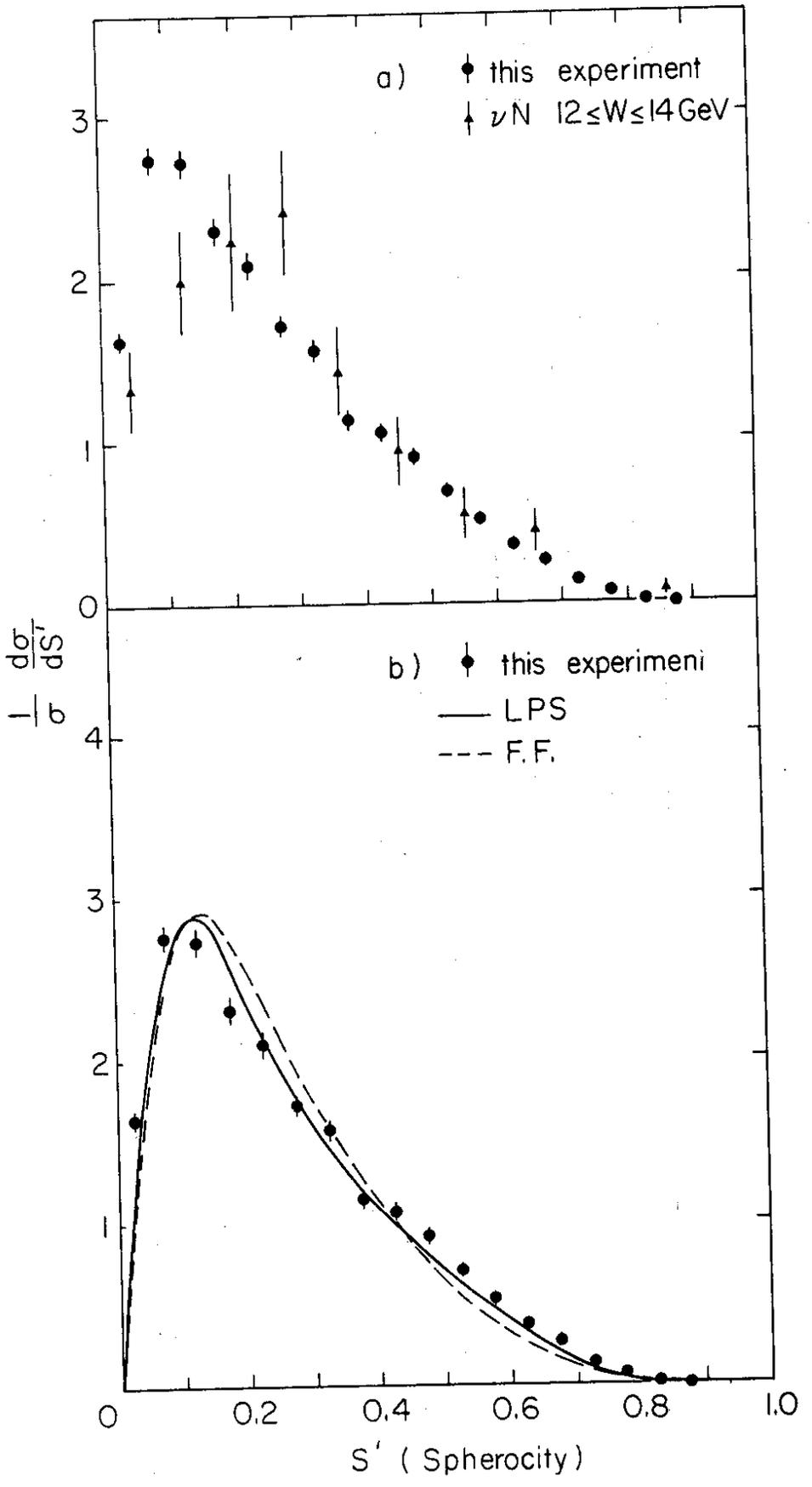
a) this experiment
νN 12≤W≤14 GeV
b) this experiment
LPS
F.F.
dσ/dS'
1/σ
S' (Spherocity)
0
0.2
0.4
0.6
0.8
1.0

Fig. 5

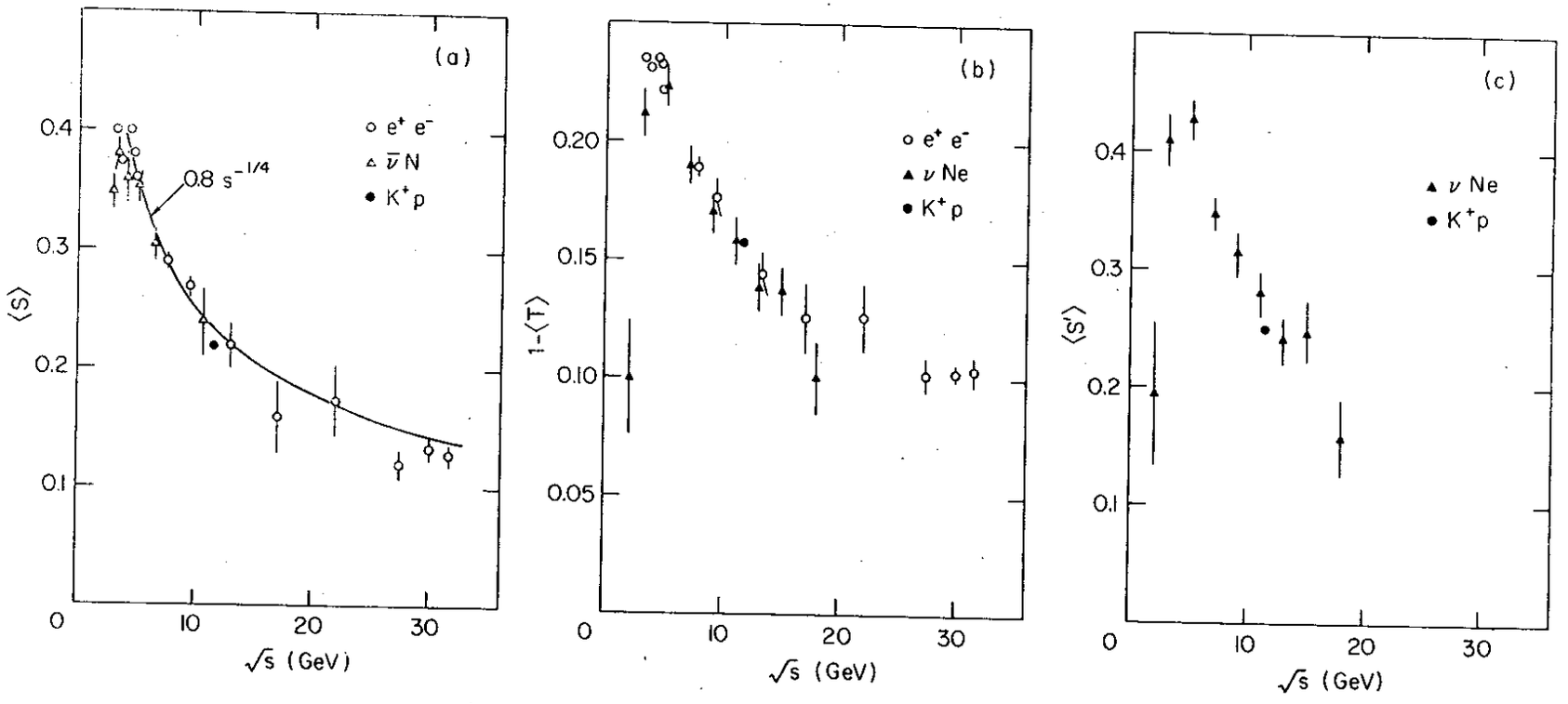
(a)
0.4
0.3
0.2
0.1
0
⟨S⟩
0.8 s^-1/4
e+ e-
ν̄ N
K+p
10
20
30
√s (GeV)
(b)
0.20
0.15
0.10
0.05
0
1-⟨T⟩
e+ e-
ν Ne
K+p
10
20
30
√s (GeV)
(c)
0.4
0.3
0.2
0.1
0
⟨S'⟩
ν Ne
K+p
10
20
30
√s (GeV)

Fig. 6

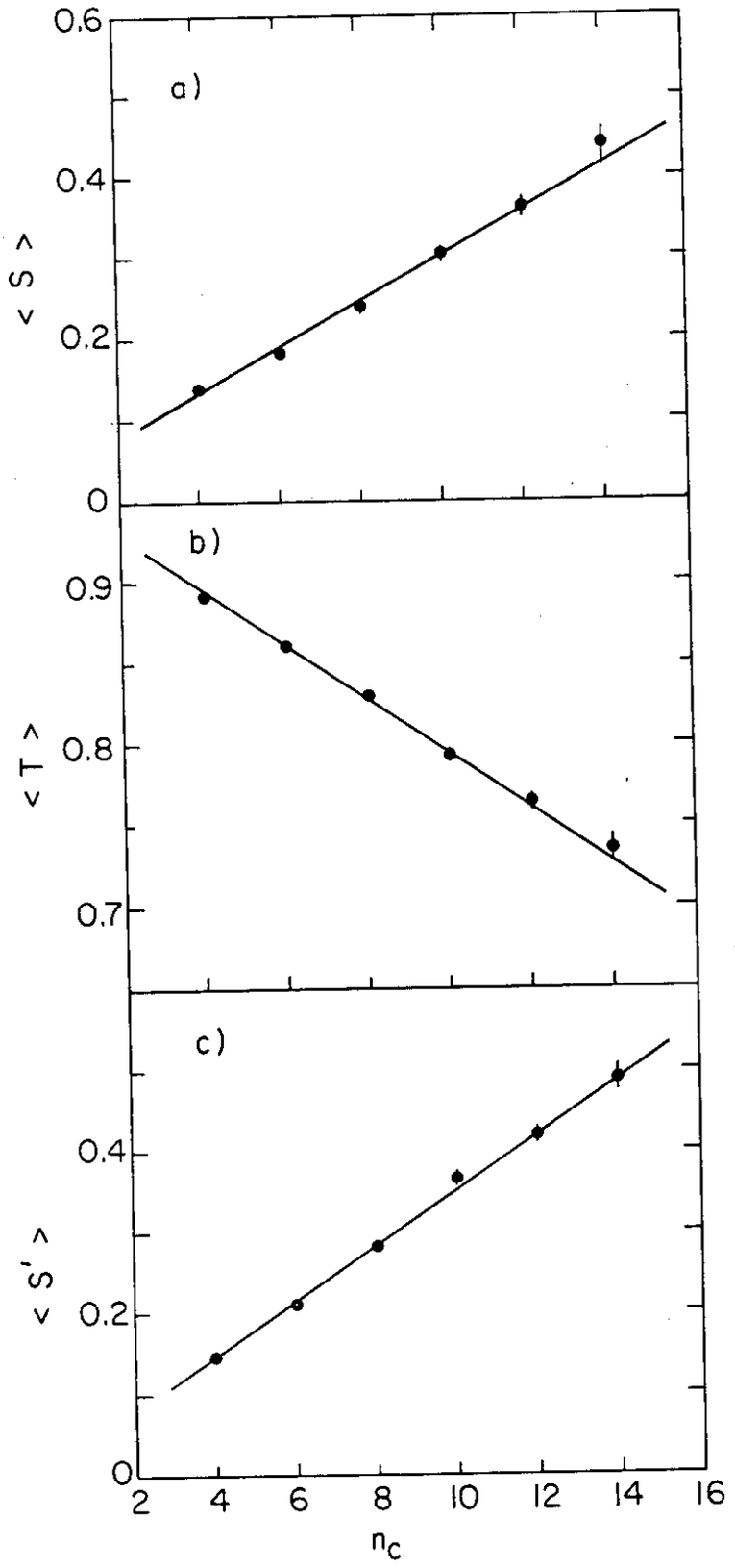

Fig. 7

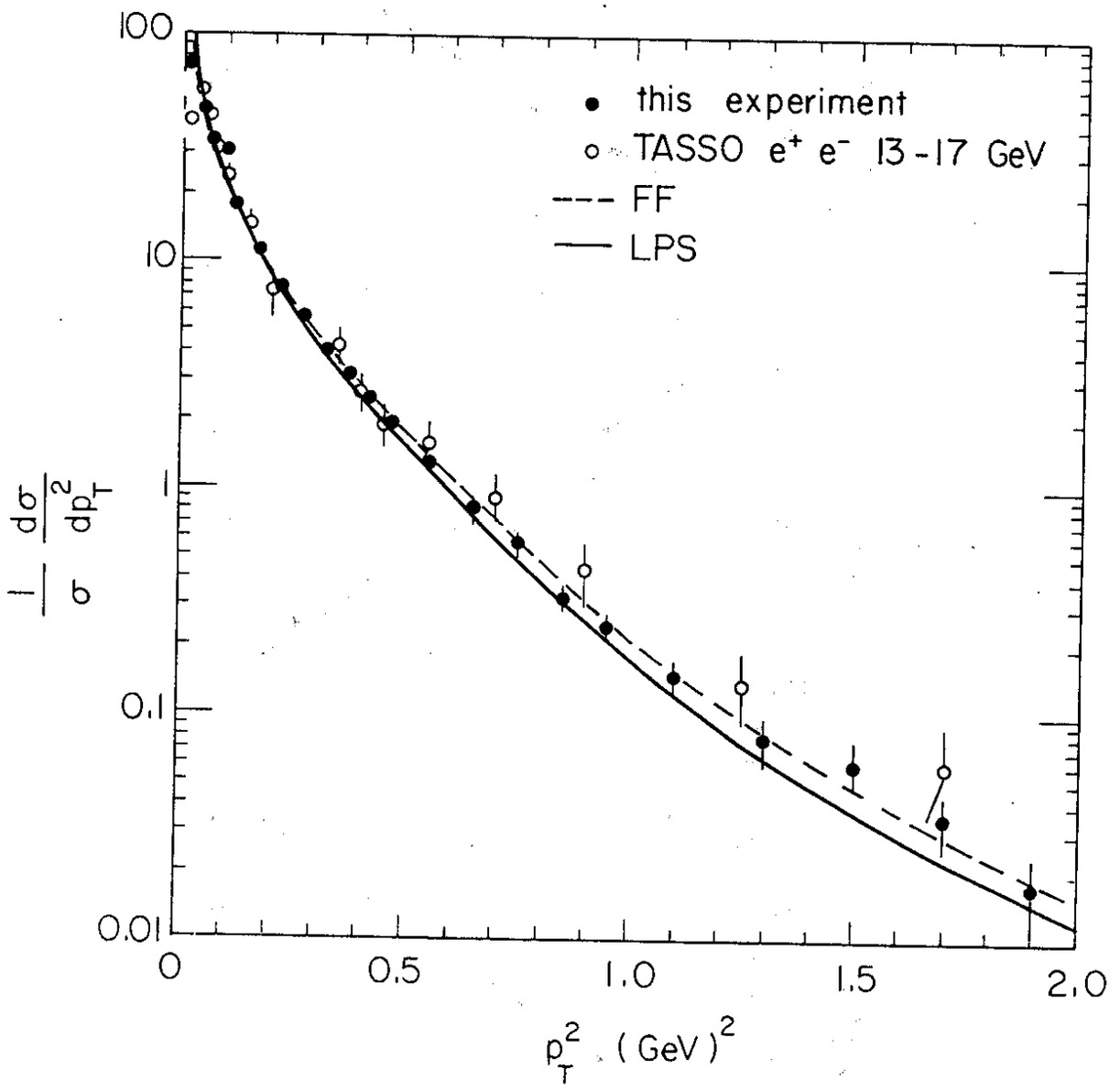
100
10
1
0.1
0.01
0
0.5
1.0
1.5
2.0
this experiment
TASSO e+ e- 13-17 GeV
FF
LPS
1/σ dσ/dp_T^2
p_T^2 (GeV)^2

Fig. 8

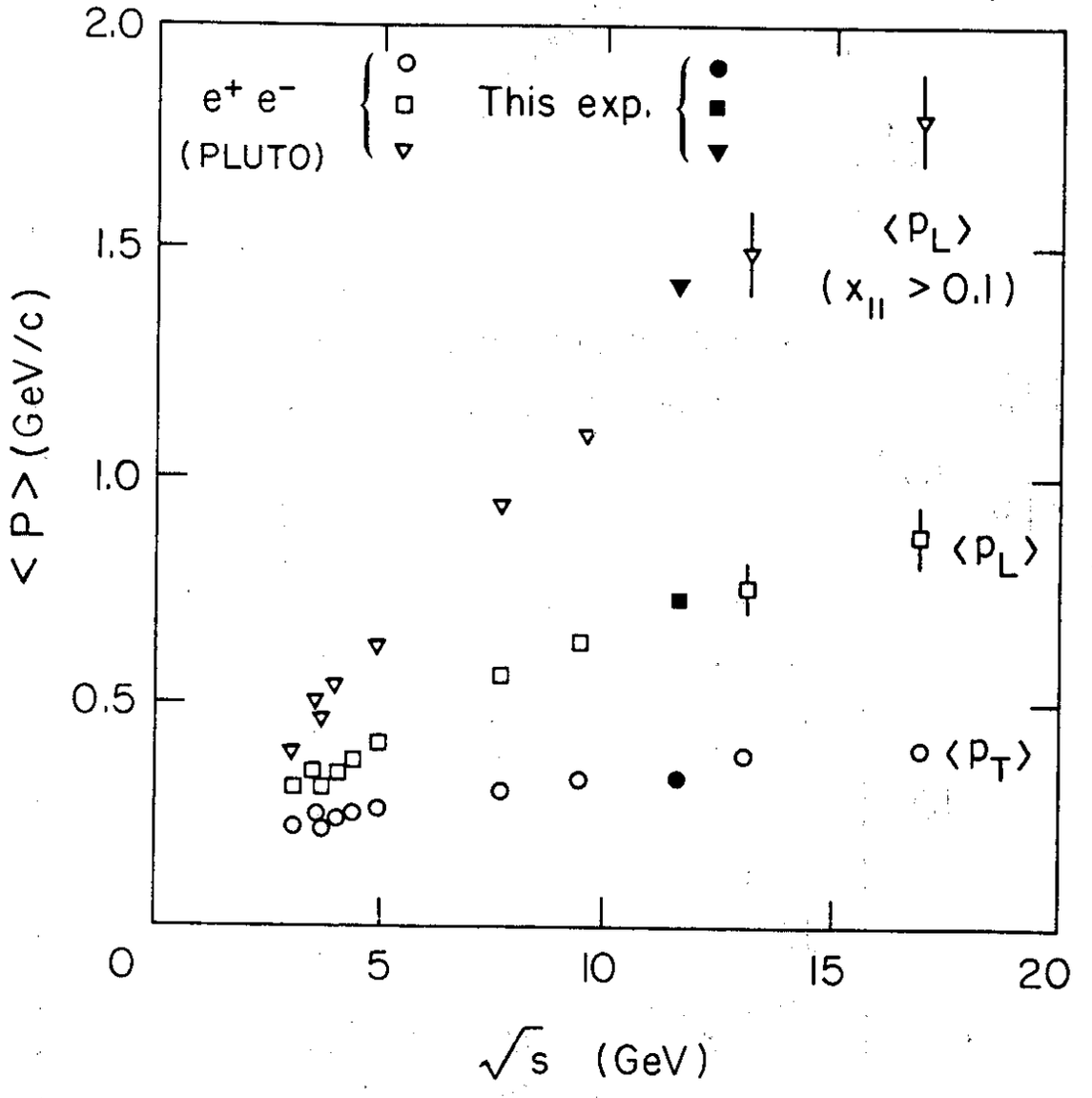

Fig. 9

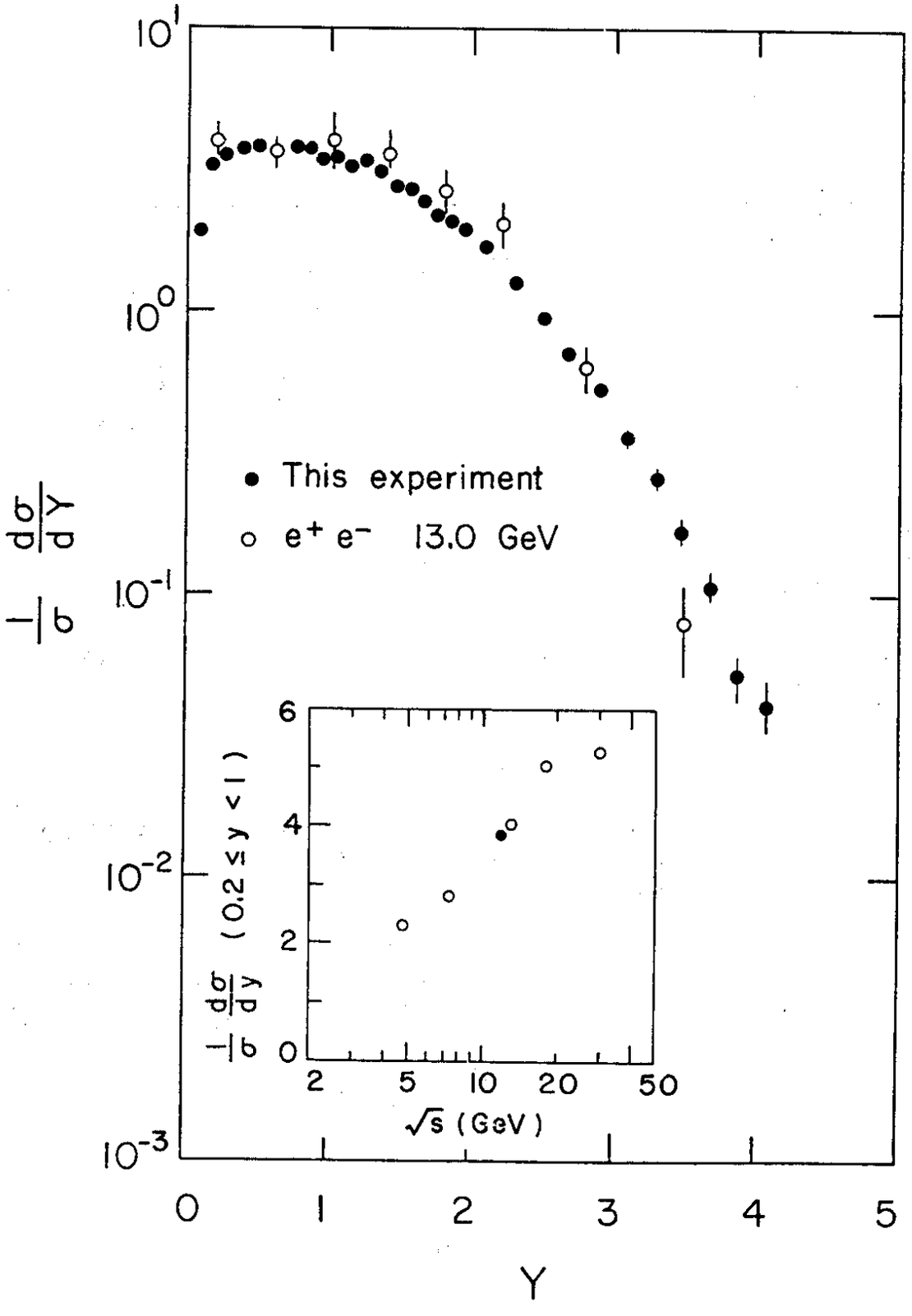
10^1
10^0
10^-1
10^-2
10^-3
dσ/dY
σ
This experiment
e+ e− 13.0 GeV
0
1
2
3
4
5
Y
6
4
2
0
dσ/dy (0.2 ≤ y < 1)
σ
2
5
10
20
50
√s (GeV)

Fig.10

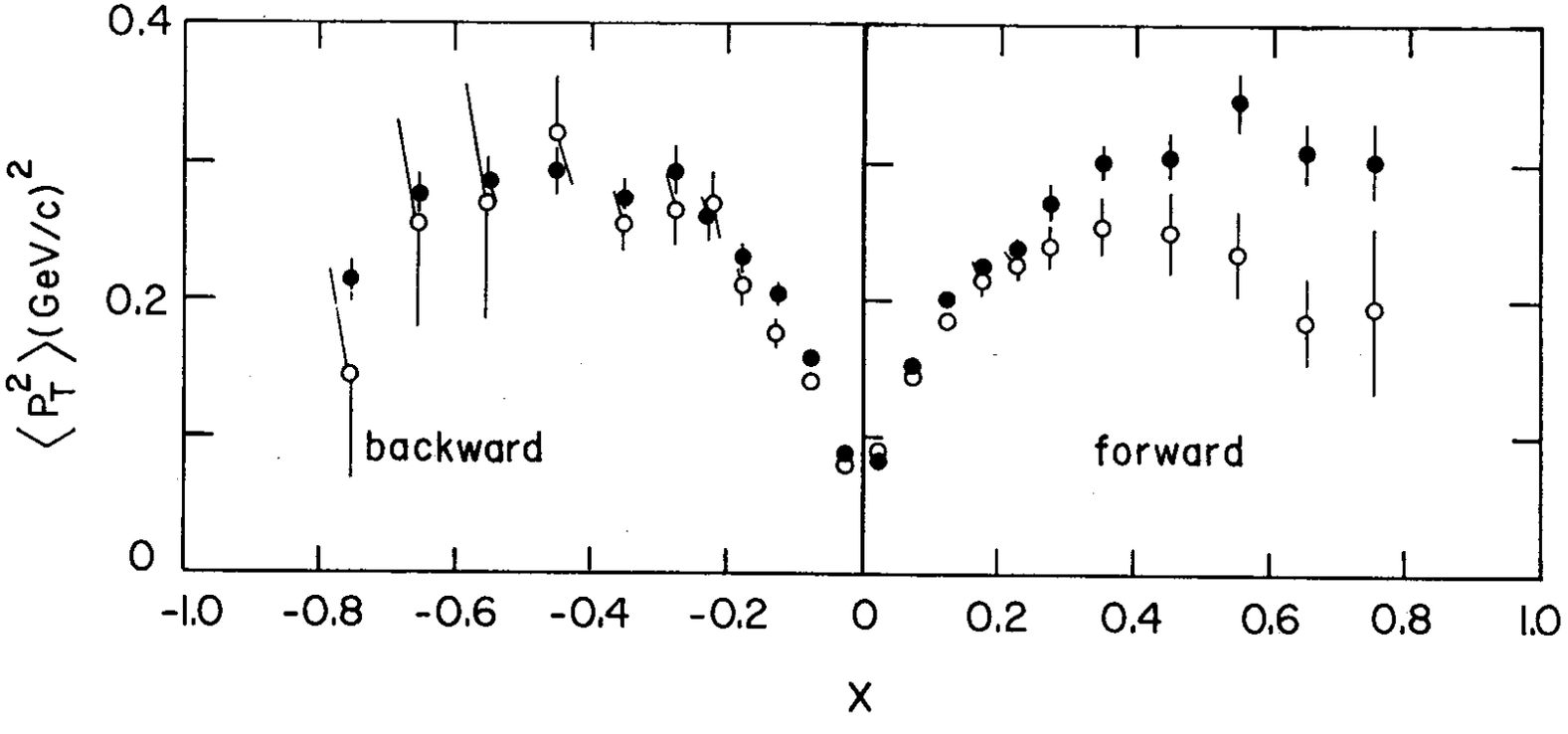
0.4
0.2
0
$\langle P_T^2 \rangle$(GeV/c)^2
backward
forward
-1.0
-0.8
-0.6
-0.4
-0.2
0
0.2
0.4
0.6
0.8
1.0
X

Fig. 11

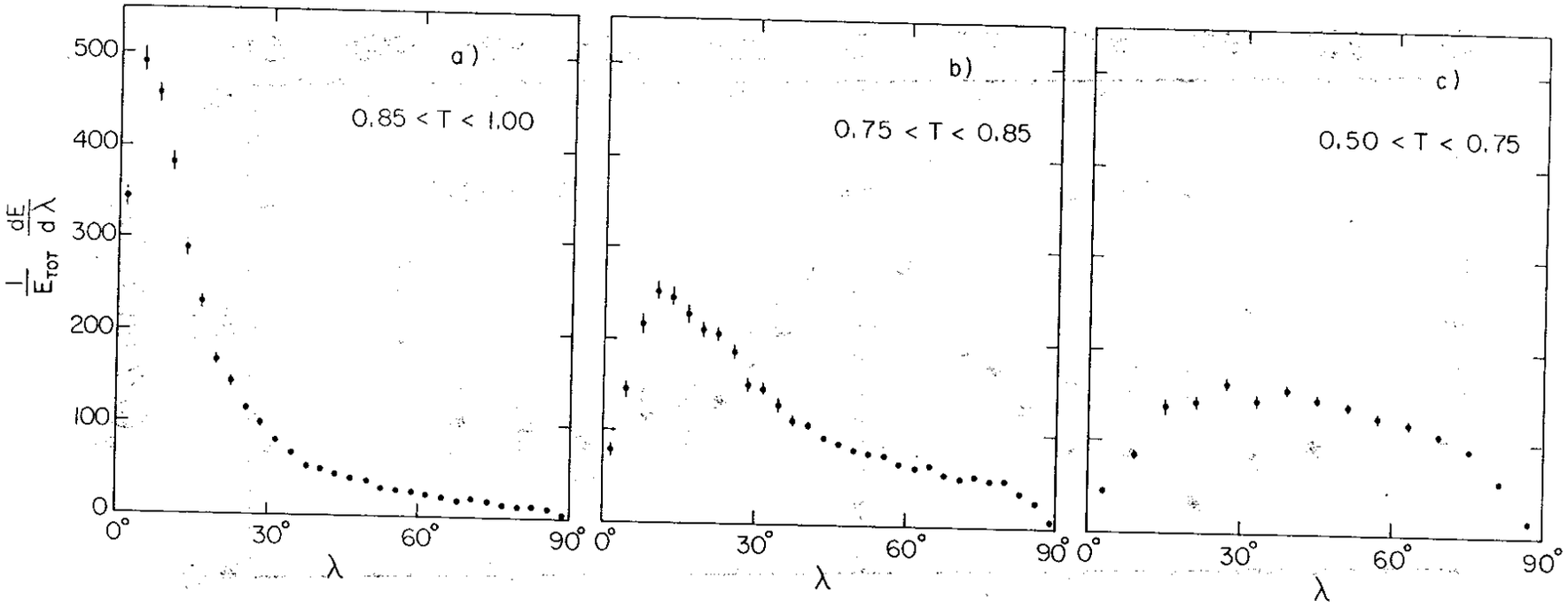
a)
0.85 < T < 1.00
b)
0.75 < T < 0.85
c)
0.50 < T < 0.75
$\frac{1}{E_{TOT}} \frac{dE}{d\lambda}$
500
400
300
200
100
0
0°
30°
60°
90°
λ

Fig. 12

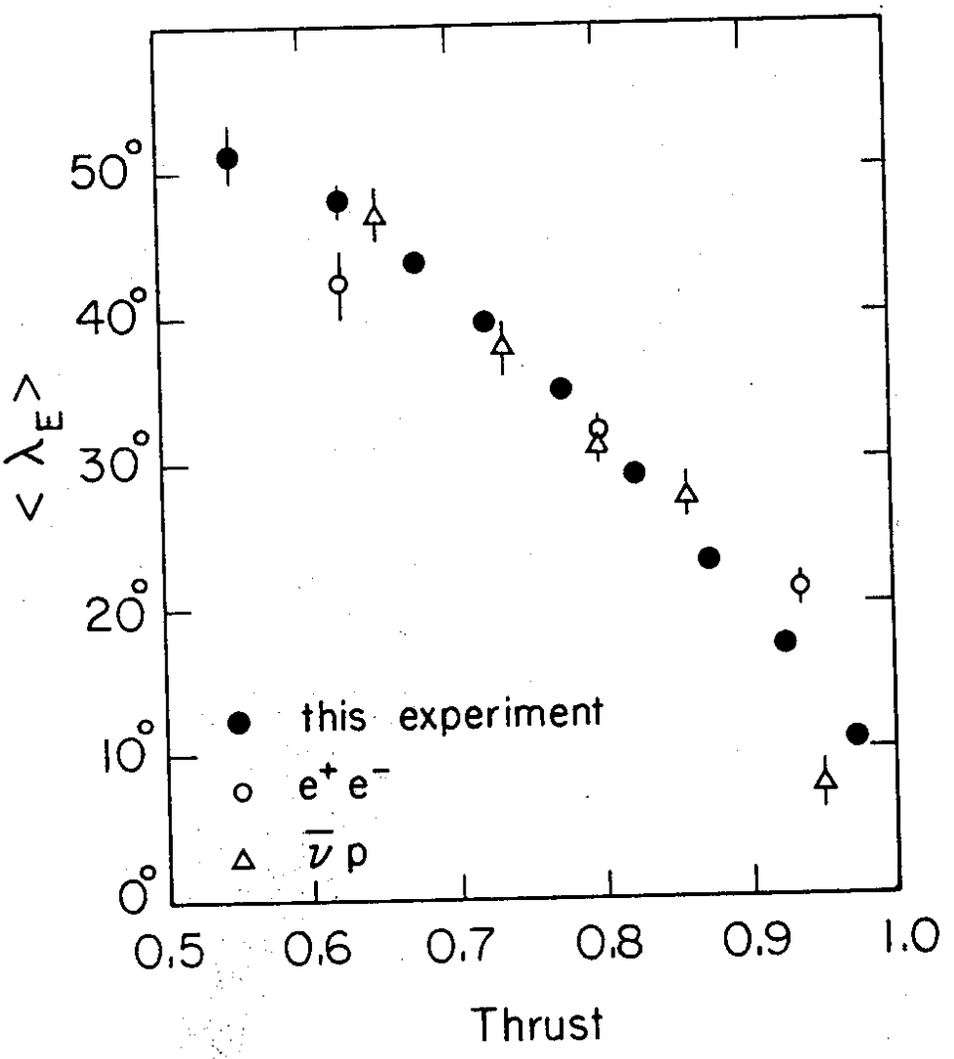

Fig. 13

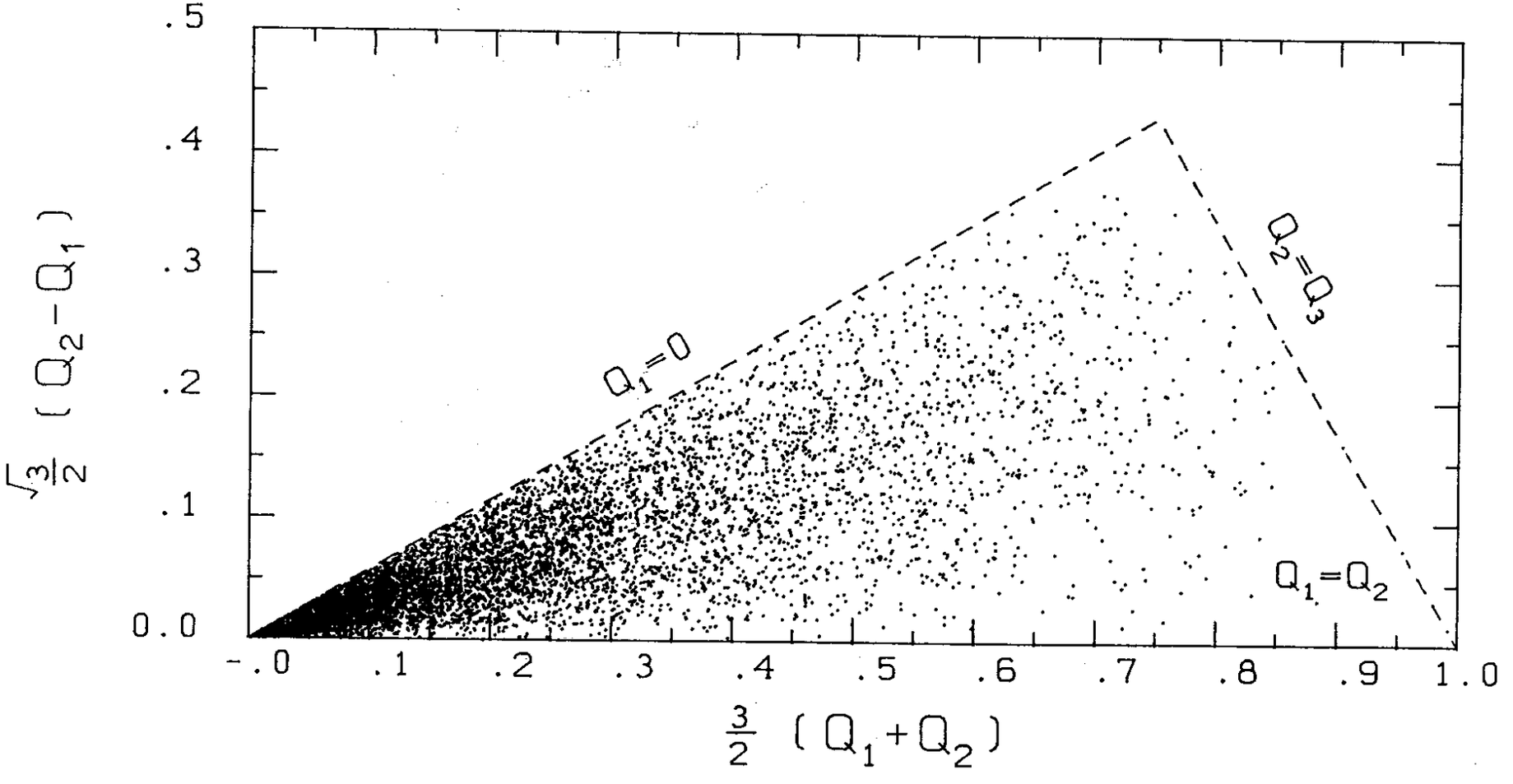
.5
.4
.3
.2
.1
0.0
-.0
.1
.2
.3
.4
.5
.6
.7
.8
.9
1.0
$\frac{\sqrt{3}}{2}(Q_2-Q_1)$
$\frac{3}{2}(Q_1+Q_2)$
$Q_1=0$
$Q_2=Q_3$
$Q_1=Q_2$

Fig. 14

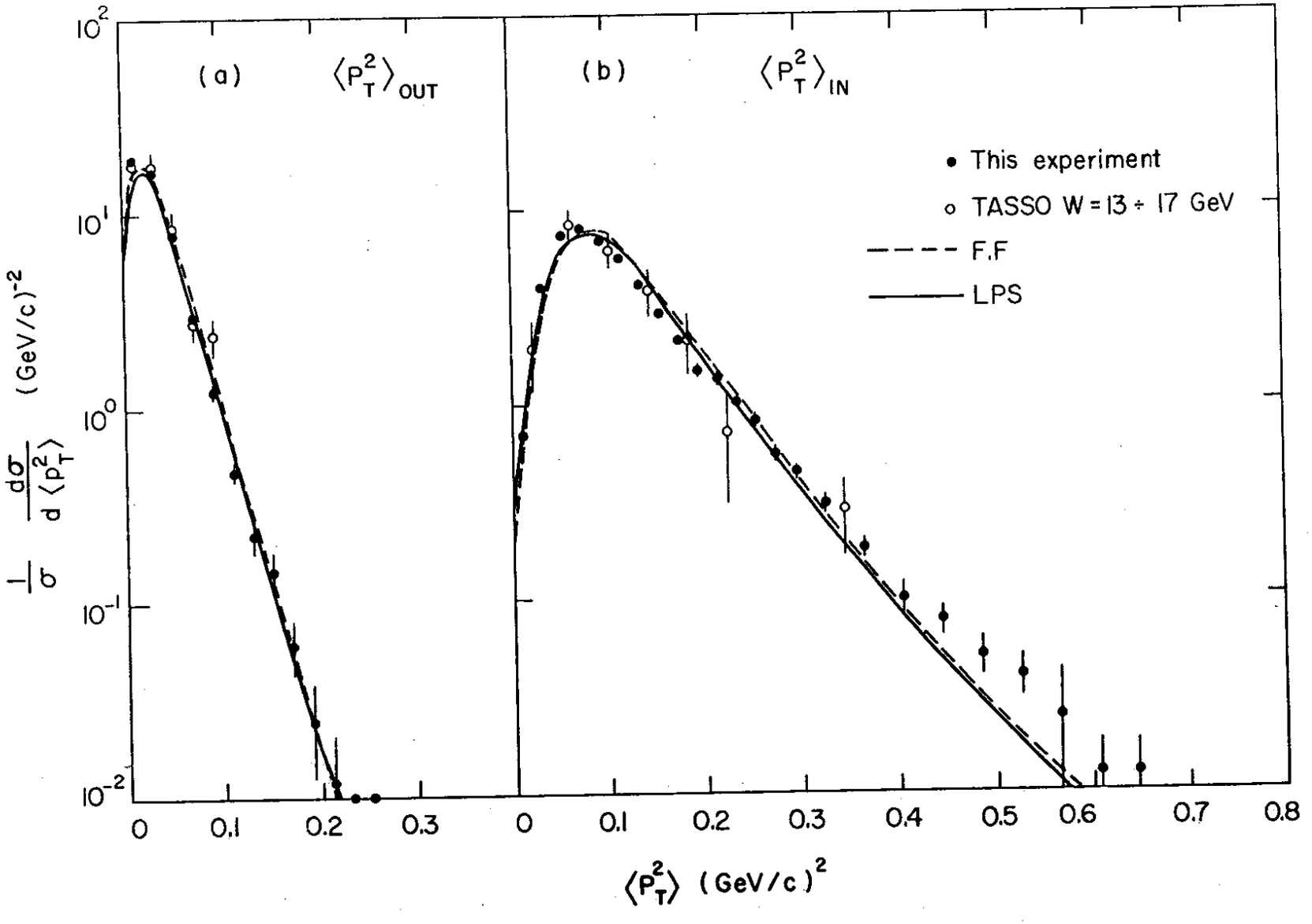
(a) $\langle P_T^2 \rangle_{OUT}$
(b) $\langle P_T^2 \rangle_{IN}$
• This experiment
○ TASSO W = 13 ÷ 17 GeV
F.F
LPS
$\frac{1}{\sigma} \frac{d\sigma}{d\langle p_T^2 \rangle}$ (GeV/c)$^{-2}$
$\langle P_T^2 \rangle$ (GeV/c)^2
10^2
10^1
10^0
10^{-1}
10^{-2}
0
0.1
0.2
0.3
0.4
0.5
0.6
0.7
0.8

Fig. 15

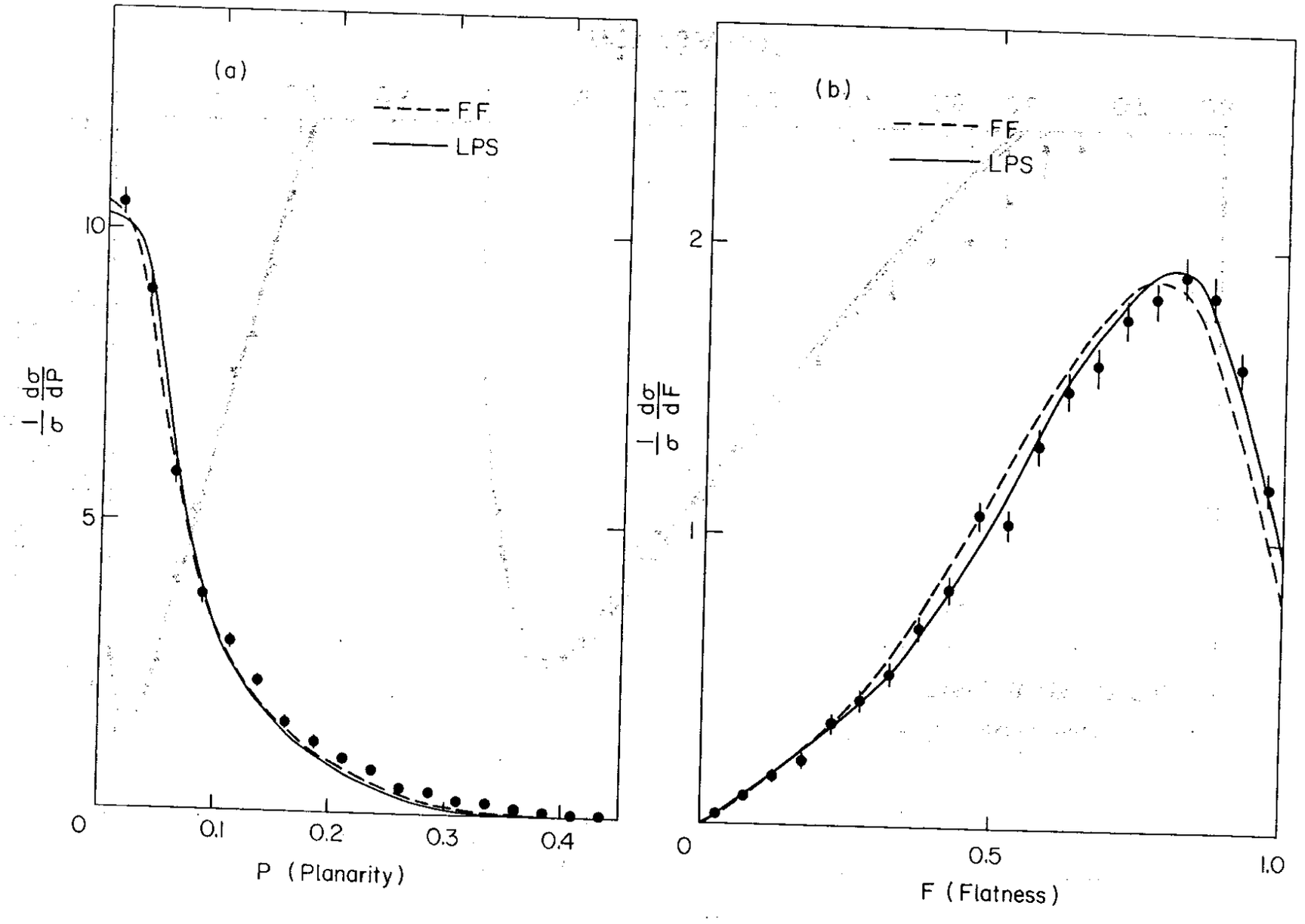
(a)
FF
LPS
10
5
0
0.1
0.2
0.3
0.4
P (Planarity)
(b)
FF
LPS
2
1
0
0.5
1.0
F (Flatness)

Fig. 16

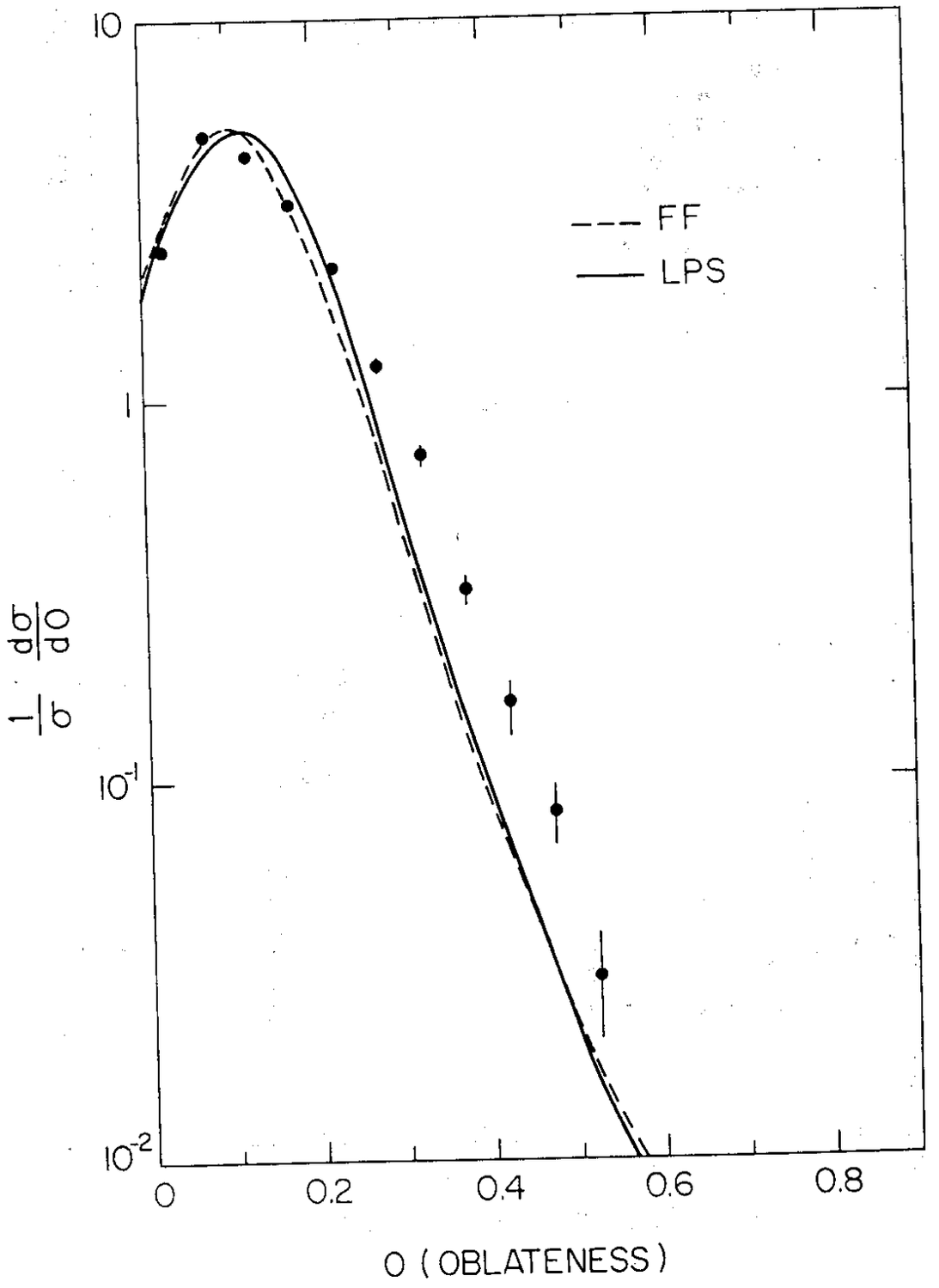
10
1
10^{-1}
10^{-2}
$\frac{1}{\sigma}\frac{d\sigma}{dO}$
--- FF
—— LPS
0
0.2
0.4
0.6
0.8
O (OBLATENESS)

Fig. 17

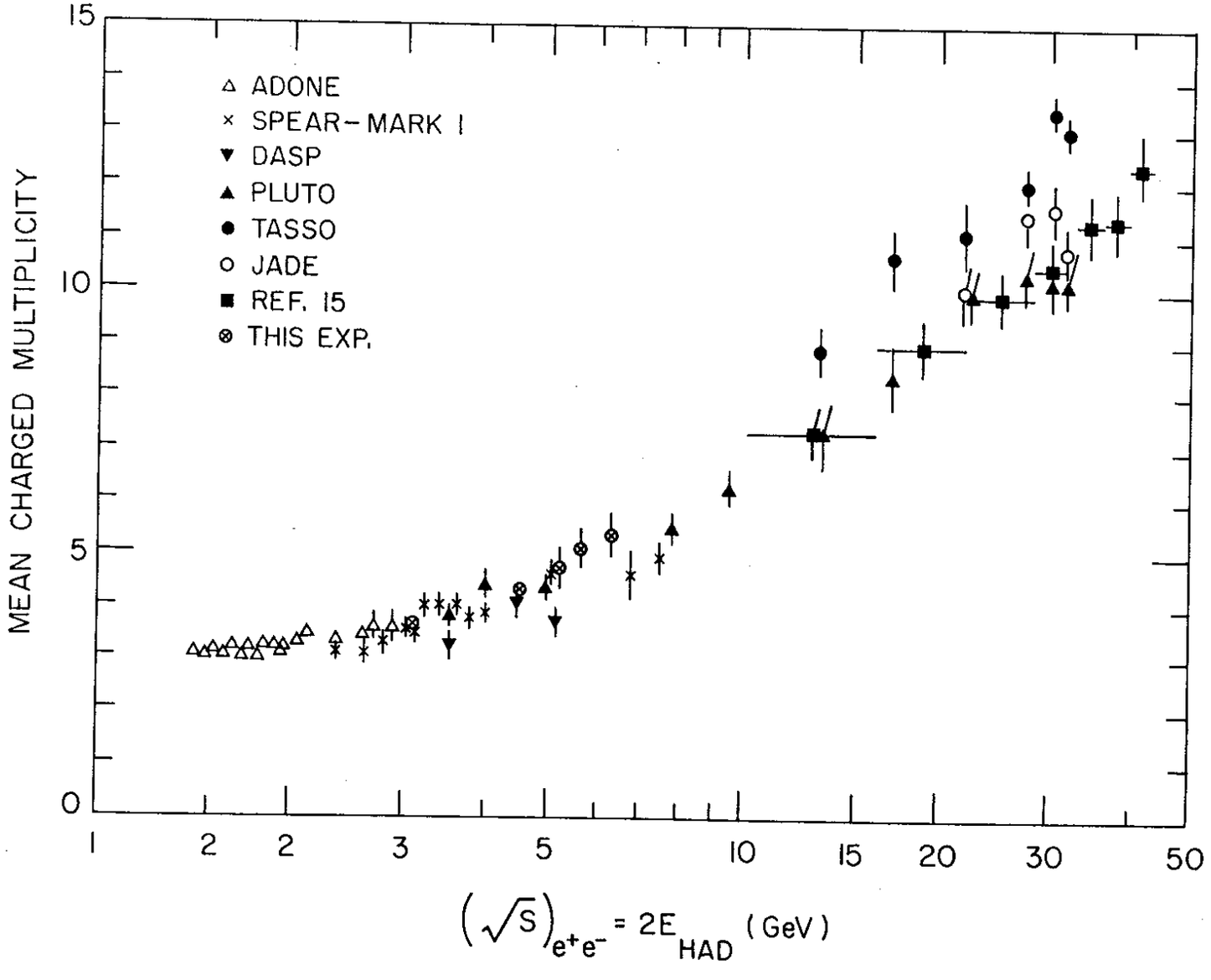
MEAN CHARGED MULTIPLICITY
15
10
5
0
ADONE
SPEAR–MARK I
DASP
PLUTO
TASSO
JADE
REF. 15
THIS EXP.
1
2
2
3
5
10
15
20
30
50
$(\sqrt{s})_{e^+e^-} = 2E_{HAD}$ (GeV)

Fig. 18

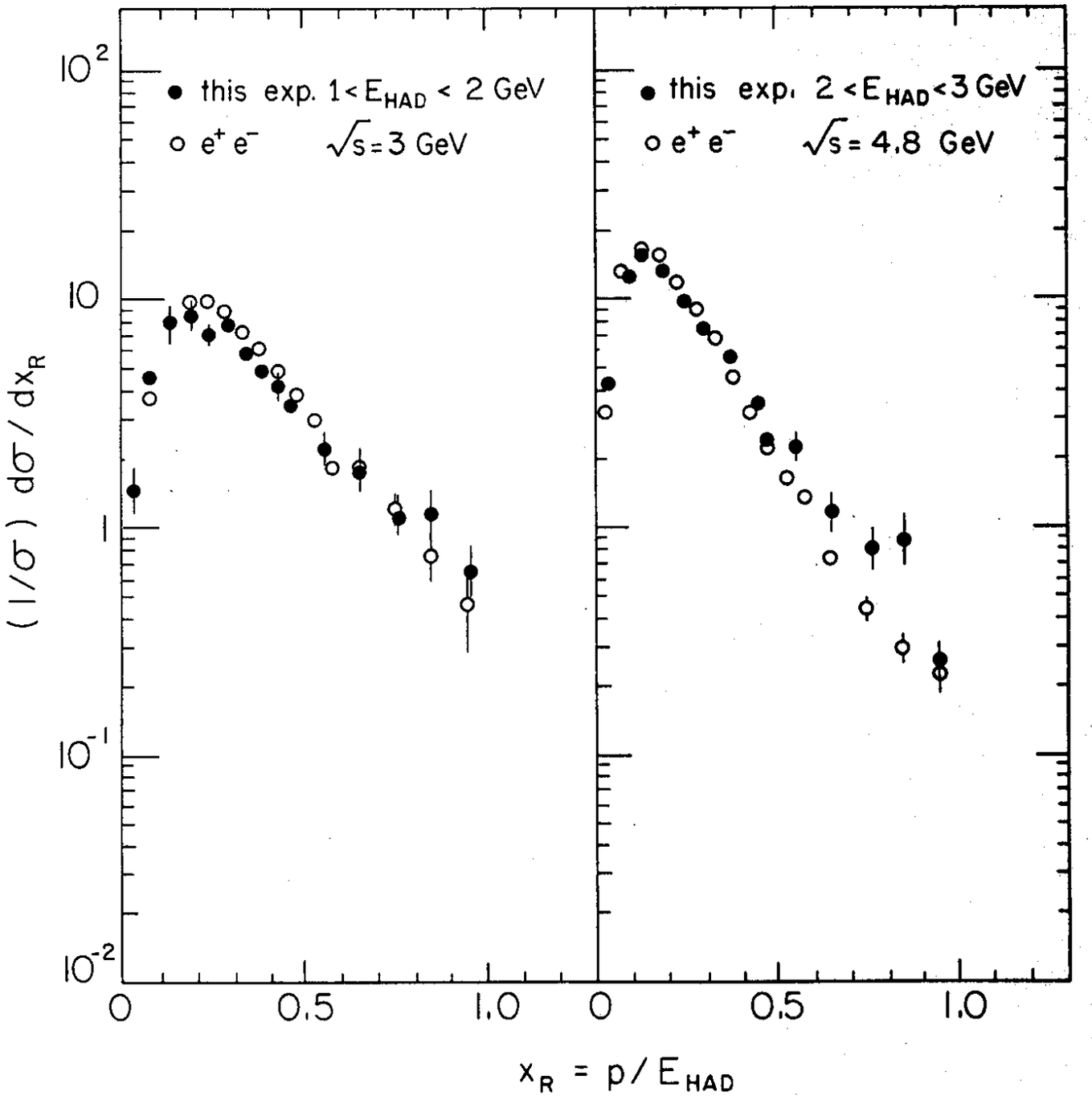
this exp. 1 < E_HAD < 2 GeV
e+ e− √s = 3 GeV
this exp. 2 < E_HAD < 3 GeV
e+ e− √s = 4.8 GeV
(1/σ) dσ/dx_R
x_R = p/E_HAD
10^2
10
1
10^-1
10^-2
0
0.5
1.0

Fig. 19